TOWARDS SPATIAL AND TEMPORAL SNOW DISTRIBUTION ESTIMATES OVER THE MOUNTAIN REGION OF THE WESTERN UNITED STATES

by

Naoki Mizukami

A dissertation submitted to the faculty of
The University of Utah
in partial fulfillment of the requirements for the degree of

Doctor of Philosophy

Department of Civil and Environmental Engineering

The University of Utah

December 2011

THE UNIVERSITY OF UTAH GRADUATE SCHOOL

STATEMENT OF DISSERTATION APPROVAL

The dissertation of Naoki Mizukami

has been approved by the following supervisory committee members:

Steven J. Burian	, Chair	6/15/2011 Date Approved
Christine A. Pomeroy	, Member	6/15/2011 Date Approved
Larry Reavely	, Member	6/15/2011 Date Approved
Rick Forster	, Member	6/15/2011 Date Approved
Randy Julandar	, Member	6/15/2011 Date Approved

and by Paul J. Tikalsky, Chair of the Department of Civil and Environmental Engineering

and Charles A. Wight, Dean of The Graduate School.

ABSTRACT

This dissertation examines three separate data analysis studies which sought to estimate the spatial and temporal characteristics of seasonal snowpack variables in the mountainous areas of the western United States. Research began with the analysis of historical daily snow data from Snowpack Telemetry (SNOTEL) sites, located in the mountainous areas of the western United States. Three snowpack characteristics were analyzed from a climatological perspective: snow water equivalent (SWE); snow depth (SD); and snow density, all three being interrelated. Analysis of 7 years of data showed that at a given location, during the winter season, interannual snowpack density variability was smaller than the corresponding SD and SWE changes. Hence, reliable climatological estimates of snow density could be obtained from a relatively short record period. Additionally, the spatial pattern of snowpack densification was qualitatively characterized using cluster analysis. The second part of research developed a regional regression-based approach to creating monthly climatological SWE grids over the western United States. The western United States was partitioned into smaller, homogenous regions in consideration of seasonal snowpack accumulation and ablation processes. Using stepwise regression, various geographic and meteorological variables were investigated as potential predictors of change in climatological SWE within each subregion. Results indicate that a simple regional regression approach, coupled with readily available geographic and meteorological parameters as predictors, is reliable for mapping SWE climatology from October to March. For the period of April, however, the regional equations produced increased error, especially in the North Pacific and Southwest regions. Lastly, performance of space-borne passive microwave

SWE retrieval algorithms for the Colorado River Basin was examined by comparing daily SWE estimates from selected algorithms with SNOTEL SWE measurements for each winter month.

Dedicated to you without saying your name

"It is one of our most exciting discoveries that local discovery leads to a complex of further discoveries."

– R. Buckminster Fuller

CONTENTS

LIST OF FIGURES

LIST OF TABLES

ACKNOWLEDGMENTS

I would like to thank all of those who helped complete this dissertation.

First, I wish to express my appreciation to my academic advisor, Dr. Steven J. Burian, for his support and advice on completion of my dissertation. Also, I would like to thank my committee members Drs. Christine Pomeroy, Larry Reaveley, Rick Forster and Randy Julandar for their very helpful insights, comments and suggestions. Sincere thanks go to Dr. Sanja Perica for encouragement, patience, and providing professional and technical advice throughout my PhD. Additionally, I would like to acknowledge the following colleagues at NWS Office of Hydrologic Development, who provided constructive discussions and comments that improved the manuscripts for the journal articles: Brian Cosgrove, James Brown, Satish Regonda, and Kevin He. I would like to thank Michael Smith of NWS/OHD and Robert Brown of Len Technologies for their consistent encouragement.

The work presented in Chapters 2 and 3 was supported in part by the University of Utah SEED grant and by the National Oceanic and Atmospheric Administration, Climate Prediction Program for the Americas grant.

CHAPTER 1

INTRODUCTION

1.1 Significance of seasonal snow pack

Seasonal snow cover is the most rapidly fluctuating cryospheric variable on the earth surface [*ACIA*, 2005]. Its extent varies from less than 1 million km^2 in summer to 40-50 million km^2 in midwinter over the Northern Hemisphere. Within North America, it can cover over 14 million km^2, equivalent to 50% of the land surface, at peak time, concentrated in the mountainous areas. Such a large and dynamic extent of seasonal snow cover play pivotal roles in the climate, ecosystem and hydrologic system.

One of the most documented roles of seasonal snow cover is its influence on the climate system. *Cohen and Rind* [1991] described many of its first-order effects. These are high albedo acting as a reflector of solar energy, low thermal conductivity, high thermal emissivity and latent heat sink during snowmelt, thus controlling surface energy balance in lower atmosphere over large land areas, and in turn affecting atmospheric circulation patterns.

Early observational studies found that snow cover can decrease the temperature of the lower atmosphere (up to 500 hPa) locally by several degrees over days to months [*Wagner*, 1973; *Dewey*, 1977], supported by subsequent modeling studies by *Walsh et al.* [1982]; *Walsh and Ross* [1988]. This suppressed atmospheric temperature is related to large-scale atmospheric circulation modes such as the Pacific-North American (PNA) and Pacific Decadal Oscillation (PDO) patterns. Over broad regional/continental scales, the bulk of the scientific literature has primarily focused on

relationships between climate and snow cover extent, namely the presence or absence of snow on land. Numerous statistical and modeling studies revealed that large continental-scale snow extent anomalies could contribute to considerable variations in atmospheric circulation via modification of the energy budget in the lower atmosphere [e.g., *Leathers and Robinson*, 1993; *Cohen and Entekhabi*, 1999; *Gong et al.*, 2002, 2003; *Saito and Cohen*, 2003; *Saunders et al.*, 2003; *García-Herrera and Barriopedro*, 2006].

More recently, *Sobolowski and Frei* [2007] reported statistical relationships between various winter climate modes and continental-scale snow pack depth (SD). At more regional scales, point observations over North America have been used to deduce statistical relationships between SD and climate over selected regions. Most of these works were based on observations over the western United States and demonstrated the effects of precipitation and temperature variability on snow volume [*McCabe and Dettinger*, 2002; *Jin et al.*, 2006; *Mote*, 2006]. *Sobolowski and Frei* [2007] detected teleconnection between summer/fall climate indices (i.e., PDO, North Atlantic Oscillation, and El-Nino Southern Oscillation) and winter snow volume over north central to western U. S. *Ge and Gong* [2009] indicated SD anomalies over North America exhibited stronger and more robust statistical relationships with large-scale climate indices compared to snow extent anomalies. They reported that zero-lag correlations between monthly average SD and PNA were statistically significant from November through April, and March and April average SD was significantly correlated with PNA in the preceding winter months, which is consistent with previous findings of a winter PNA and April 1st snow volume relationship [*Jin et al.*, 2006]. However, studies on the contribution of the SD to climate variability have been much less extensive largely owing to the lack of spatially and temporally broad SD datasets.

The ecological impacts of seasonal snow cover are also noteworthy. Seasonal snow

cover is one of the most important environmental factors controlling plant growth in the alpine tundra ecosystem [*Billings*, 1988; *Walker et al.*, 1993] because of its direct effect on soil temperature, moisture, duration of the growing season and control of nutrient availability in the alpine environment [*Williams et al.*, 1998].

Snowpack acts as an excellent insulator of the underlying ground because of the low thermal conductivity of snow, resulting in soil temperatures up to 15 degrees warmer underneath a snow pack [*Mölders and Walsh*, 2004]. Ground temperatures beneath snow cover can be influenced as much by the snow as the overlying air temperature, as demonstrated by *Stieglitz et al.* [2003], who attribute half of the temperature rise in the 20-m soil at Barrow, Alaska to locally increasing snow cover since the 1970s. Snowpack energy balance model confirms that the insulative ability of snow pack increases with increasing SD [*Ge and Gong*, 2010]. The insulating ability of a snow pack permits a great amount of ecological activity during winter, much of which happens within the soil where temperatures can remain high enough to support a wide range of biotic activities [*Campbell et al.*, 2005]. Counterintuitively, warmer winters may actually result in colder soils because of snow cover reductions based on field studies in which snow is manually removed from test plots [*Groffman et al.*, 2001; *Decker et al.*, 2003]. The associated consequences were reported to be greater root mortality, more nutrient losses, and decreased productivity of certain tree species.

Lastly, hydrologic cycle in high-mid latitude is directly affected by the seasonal snow accumulation and ablation [e.g., *Dyer*, 2008]. Seasonal snowpack stores water during the cold months, which is then released as snowmelt runoff. In the mountainous areas of the western United States, between 40 and 70% of annual precipitation occurs in the form of snowfall, rendering accumulated snow important to water resources over the regions [*Serreze et al.*, 1999]. In response to the melt water from the seasonal snowpack, annual peak flows often occur in spring and early

summer and contribute as much as 75% of the annual runoff over the region [*Palmer*, 1988].

The significant relationships between snow storage and discharge characteristics (the magnitude and timing) have been observed in many other parts of the northern hemisphere [e.g., *Zhang et al.*, 2001; *Yang et al.*, 2003; *Dyer*, 2008]. Many studies showed that timing of snowmelt onset has become early over the recent decades, associated with warming in winter and spring air temperature in various mountainous areas across North America including Canada, Alaska, Sierra Nevada, and North Pacific [*Lammers et al.*, 2001; *Regonda et al.*, 2005; *Stewart et al.*, 2005]. This indicates a shift in a hydrologic cycle over the continent driven by changes in the snow accumulation and ablation patterns. Given this change in the seasonal snow accumulation and melt pattern, water resource managers could be faced with the challenge of predicting the timing and the amount of snowmelt runoff to optimize the management of hydropower, municipal and industrial water demand, and recreation.

In contrast to the vital roles in water resources of snow, snowmelt can cause devastating floods as well. The snowmelt driven flood is typically driven by a rain-on-snow event [*Leathers et al.*, 1998] and is a concern particularly in a maritime climate regime such as the North Pacific [*Hall and Hannaford*, 1983; *Marks et al.*, 1998].

To this end, snow volumetric variables are most needed in various temporal and spatial scales to better understand and model earth climate, ecosystem, and hydrologic cycle in snowy areas. The next subsection describes measurement methods for snow volumetric variables.

1.2 Volumetric snowpack variables and measurements

Both snow water equivalent (SWE) and SD represent the volumetric quantities of snow pack. SD is a thickness of snow pack from the bottom to the surface of the pack

while SWE is a mass of snow pack column within a unit area. SWE is more widely used for hydrology applications as it also represents the amount of water snow pack yields if it melts completely. SWE (cm) is related to snow pack density (kg/m^3) and SD (cm) through the following relationship:

$$SWE = SD\frac{\rho_s}{\rho_w} \tag{1.1}$$

where ρ_s is the density of snow pack in kg/m^3, ρ_w is the density of liquid water (approximately 1000 kg/m^3 at 0 C). This relationship allows one to convert SD to SWE or vice versa given snow pack density.

The most traditional but accurate method, manual snowpack measurements, also known as a snow survey, can be made using a hollow snow tube for sampling of a snow core from the snow pack. The Federal snow samplers most typically used in the United States are made of 76.2-cm (30-inch) long aluminum tubes with an inside diameter of about 3.8 cm (1.5 inch). A snow core is sampled by vertically inserting the tube into the snow pack until it reaches the ground and then turning the tube to plug the snow at the tube base. At this point SD can be easily measured by reading a scale marked outside the tube. The tube together with the sampled snow core is weighed and then repeated without the sample to obtain a difference, or SWE. More detailed descriptions of site selection, measurement tools, and measurement procedure can be found in *Goodison et al.* [1981].

In the western U.S., systematic manual snow surveys have been performed at predetermined snowcourse by Soil Conservation Service (SCS, currently The Natural Resources Conservation Service; NRCS) since the 1930s for water supply forecasting purpose. Each snowcourse consists of approximately 10 measurement points marked by stakes. The snow surveyor can return to the site periodically, once or twice a month during the snow season [*Dunne and Leopold*, 1978]. A traditional method in predicting spring stream discharge uses an empirical model developed based on

such point SWE measurements made within a basin and its corresponding discharge measurements in the stream [*United States Army Corps of Engineers*, 1956].

In the mid 1960s, NRCS started installing an automated system called SNOpack TELemetry (SNOTEL). This measurement system was designed to collect near-real time snowpack and related climatic data (air temperature and precipitation) over the western U.S. including Alaska in places where previous NRCS historic snowcourse data correlated well with streamflow volumes [*Schaefer and Johnson*, 1992] and at remote locations that are particularly difficult to access. At each SNOTEL site, a fluid-filled pillow is installed under the ground. Snow mass or SWE is measured by reading hydrostatic pressure produced by snow accumulated over the pillow. The collected data are transferred via a meteor burst communication technology to a master station where the data are made available to the public. SNOTEL sites are less frequent at elevations above tree lines, at low elevations and south facing terrain. Although some sites have measurements as early as the 1964 winter season, data at most SNOTEL sites became available starting in the late 1970s. The number of SNOTEL sites increased drastically in the 1980s, and presently there are close to 700 sites across the western U.S. (Figure 1.1). In the mid 1990s, NRCS started installing ultrasonic snow depth sensors at a few SNOTEL sites to measure SD in addition to SWE. The number of sites reporting both, SWE and SD, has increased significantly since then. Currently over 500 sites are reporting both snow properties (Figure 1.1).

1.3 Methods of snow distribution estimate

1.3.1 Statistical interpolation of point measurements

Information on spatially distributed snow variables, rather than point datasets, is of more interest for recent hydrologic and climate studies. For example, such information is in demand for the distributed model application over snow dominated areas [e.g., model evaluation, initialization, and update; *Dressler et al.*, 2006].

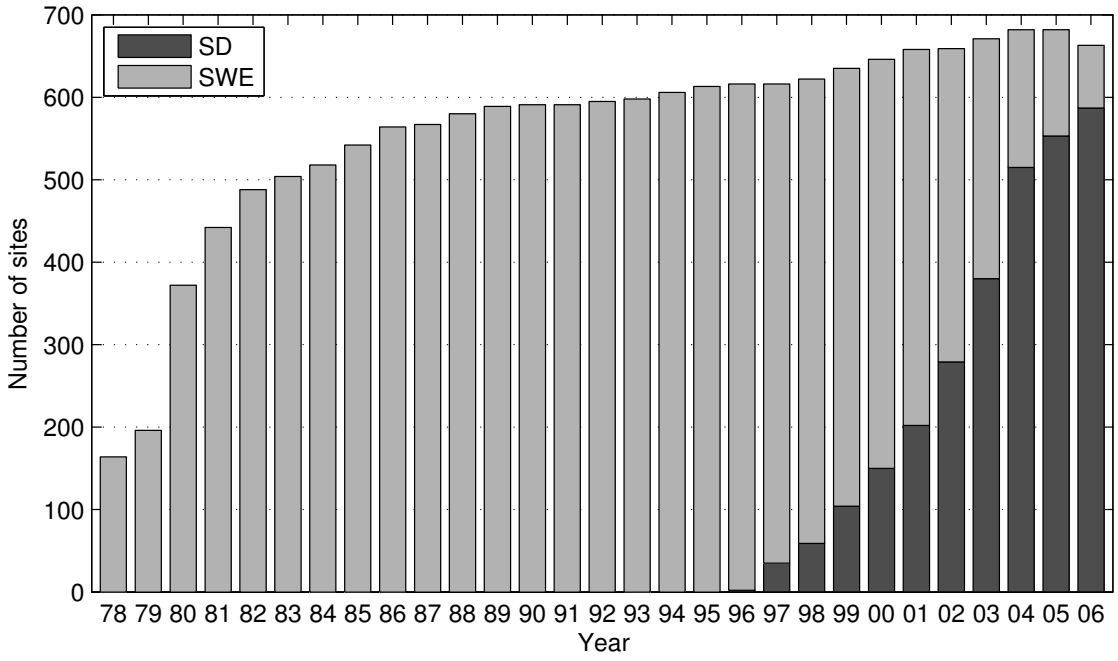

Figure 1.1. The number of SNOTEL sites reporting snow depth and snow water equivalent. Alaska sites were excluded.

Statistical models using various independent variables (e.g., topographic data) as predictors are the most common methods to interpolate point SWE or SD measurements at ungauged locations. Various geostatistical techniques such as kriging [*Hosang and Dettwiler*, 1991; *Carroll and Cressie*, 1997; *Balk and Elder*, 2000; *Erxleben et al.*, 2002; *Erickson et al.*, 2005], or binary regression tree [*Elder et al.*, 1998; *Balk and Elder*, 2000; *Erxleben et al.*, 2002; *Anderton et al.*, 2004] have been used. Many of these studies showed that coupling two statistical interpolation methods yielded the improved accuracy, e.g., applying the binary regression tree to the residuals from generalized additive model [*Moreno et al.*, 2010] or kriging to binary regression tree model [*Balk and Elder*, 2000; *Erxleben et al.*, 2002]. All of the above studies examined spatial variability of SWE or SD over a headwater basin (up to 100 km^2). Within such areal extent, heterogeneous snowmelt pattern caused by heterogeneous incident solar radiation, snow redistribution by heterogeneous wind field and snow avalanche, and elevation variation of air temperature are major derivers of physical processes of snow distribution. The scale of such physical processes of snow distribution can be by far less than 100 meter. Therefore, a measurement scale [space between measurement points; *Blöschl*, 1999] has to be smaller than this physical process scale to depict the spatial structure of SWE or SD variability (e.g., variogram). So does the model scale [spatial resolution; space between interpolation points; *Blöschl*, 1999] to map realistic spatial distributed SWE or SD fields for this areal extent. However, such dense measurements are normally available only through labor-intensive snow surveys, and therefore are usually performed for a limited time and basin.

Compared to the small headwater basin studies, only a few studies attempted spatial interpolation of operational ground SWE measurements over larger areas where intensive snow surveys are not feasible. Identifying the physiographic effects

on SWE distribution processes over larger basins (e.g., > 1,000 km^2) is particularly challenging [*Molotch and Bales*, 2006] probably due to lack of an extensive and dense snow data set to examine this. However, the snow processes at less than 100 m scale may not be important for SWE distribution over the larger extent, where a model scale used is typically above 1 km. A hypothesis used in the past studies below is that the large scale (>1 km) elevation and other physiographic characteristics [*Fassnacht et al.*, 2003] control SWE distribution at such scales. *Daly et al.* [2000] used the hypsometry-detrending regression technique to interpolate SWE measurements over the San Joaquin and Sacramento River basins in the Sierra Nevada, California. *Fassnacht et al.* [2003] tested multivariate regression, inverse distance weighting and elevation-detrended regression-inverse distance weighting techniques to estimate daily SWE at 1-km resolution for three winter season types (average, wet, and dry) over the Colorado River basin. *Fassnacht et al.* [2003] indicated that regression-based techniques could produce reliable SWE estimates over large areas during snow accumulation seasons, but that error magnitudes become significantly larger during snowmelt seasons. More investigations on the SWE distribution over the large scale (>1 km resolution) and areal extent (>1,000 km^2) will be required to understand and model the SWE distribution process.

1.3.2 Remote sensing

Besides direct ground SWE measurements conjunction with the spatial interpolation, SWE distribution can be estimated indirectly from remotely sensed data (e.g., microwave and gamma).

Airborne gamma radiation SWE surveys, such as the one operated by the National Weather Services National Operational Hydrologic Remote Sensing Center [*Carroll*, 2001], can provide reliable mean areal SWE estimates along flight lines [approximately 10 km x 300 m; *Cline et al.*, 2009]. However, this approach may not be feasible when

continuous estimates of SWE over large areas are needed.

Satellite observation is more suitable for spatially and temporally continuous monitoring snow pack in regional to global scale. This is beneficial particularly for remote mountainous areas or high latitude where the ground measurements are not available, and very difficult or costly to conduct. The National Oceanic Atmospheric Administration, National Environmental Satellite, Data, and Information Service have been operationally producing snow cover maps for Northern Hemisphere using visible range image from the satellite for four decades [*Ramsay*, 1998]. Besides the snow cover area mapping, various studies investigated retrievals of snowpack condition such as grain size, liquid water content and impurities using imageries from visible through near-infrared range of electromagnetic spectral [0.4 μm through 2.5 μm; *Dozier and Painter*, 2004]. However these observations are limited to top portion of snowpack because the penetration depth of light in visible/near infrared spectrum is very shallow [e.g., 0.5 mm in visible range and only a few millimeters in near- mid infrared spectrum; *Dozier and Painter*, 2004].

In contrast, a microwave radiation (1 mm to 1,000 mm wavelengths; 0.3 GHz to 300 GHz frequencies) can penetrates the snowpack typically 10 to 100 times of the wavelength, which is equivalent to approximately 500 to 1,000 mm of snow depth, depending on the physical snowpack properties [*Tait and Armstrong*, 1996]. Also, unlike the visible range radiation, the microwave radiation is little blocked by nonprecipitating clouds, and observations are independent of the solar illumination. Consequently, the measurements are less affected by weather conditions and are permissible during the nighttime [*Ulaby et al.*, 1986]. Brightness temperature (TB) is a measure of the radiation in terms of the physical temperature of a hypothetical black body emitting an identical amount of radiation in the same wavelengths. TB of the microwave radiation in Kelvin is given by the Rayleigh-Jeans expression:

$$\mathrm{TB} = \sigma \mathrm{T} \tag{1.2}$$

where σ is an emissivity (nondimensional number less than one) and T is a physical temperature of the snowpack in Kelvin. As the microwave radiation emitted by the underlying soil travels upward through the snowpack the microwave intensity is attenuated through absorption and volume scattering by the snow crystals. As a result, TB of the microwave radiation emanated from the snowpack is lower than snow-free areas. For the dry snow, emissivity depends primarily on the amount of volume scattering since the absorption of radiation is very low. The scattering becomes more pronounced as the grain size approaches the radiation wavelength. The amount of volume scattering also depends on the snowpack depth and fraction of the snow particles (i.e., snow density) along the emission path. Since the product of snow depth and density defines SWE, the brightness temperature reflects the amount of SWE.

Many SWE retrieval algorithms using TB observed from space-borne passive microwave radiometers have been developed over the last two decades [e.g., *Chang et al.*, 1987; *Goodison and Walker*, 1995; *Singh and Gan*, 2000; *Pulliainen and Hallikainen*, 2001; *Koenig and Forster*, 2004; *Tedesco et al.*, 2004; *Gan et al.*, 2009]. The algorithm developed by [*Chang et al.*, 1987] is among the first algorithms (hereafter the Chang's equation) and is the basis of the majority of subsequently developed algorithms. It is still used in practical applications, for example, for continental to global mapping of SWE [e.g., *Foster et al.*, 2009]. The original Chang's equation was based on TB measured from Scanning Multichannel Microwave Radiometer (SMMR; operated from1979 to1987). The equation uses TB difference between two frequency channels:

$$\mathrm{SWE} = a(\mathrm{TB}_{18H} - \mathrm{TB}_{37H}) \tag{1.3}$$

where a is a grain size coefficient that was estimated to be 4.8 mm/K for dry snowpack with constant grain size of 0.3 mm and constant snow density of 300 kg/m^3, TB_{18H}

and TB_{37H} are brightness temperatures at horizontally polarized 18 GHz and 37 GHz frequency channels, respectively. TB at higher frequency (TB_{37H}) is by far more sensitive to the volumetric scattering than TB at lower frequency (TB_{18H}), resulting in lower TB_{19H}; and by taking the difference in TB between two frequency channels, the effect of snow temperature on TB was reduced. For one of the current operational passive microwave radiometers - Special Sensor Microwave Imager (SSM/I), carried aboard Defense Meteorological Satellite Program (DMSP) satellites, provide slightly different frequency TB (19 GHz frequency channel instead of 18 GHz). However, difference between 19 and 18 GHz has a very small effect on the algorithm performance since the penetration for both frequencies is nearly identical [*Foster et al.*, 2005]. There have been inconsistencies in the selection of the polarizations (horizontal or vertical) used in the equation, but the choice of the polarization seemingly has little effect on the algorithm performance over the large scale SWE mapping [*Rango et al.*, 1979].

Among various snowpack characteristics, wet snow and depth hoar affect the accuracy of the passive microwave derived SWE estimates. In a wet snowpack, liquid water that resides inside the snowpack or on its surface alters microwave interaction with the snowpack from scatter to emission due to higher dielectric constant of the liquid water, resulting in very little brightness temperature difference between different frequency channels, and consequently making it difficult to discriminate between no-snow and wet snowpack areas. This sensitivity of the microwave to liquid water content of snowpack is useful for identification of wet and dry snow cover areas and for estimation of snowmelt timing [*Walker and Goodison*, 1993], but is undesirable for estimation of SWE.

A depth hoar is formed by recrystallization caused by water vapor transfer between snow crystals driven by strong temperature gradients within the snowpack.

In contrast to typical snow grains in a dry snowpack, which are less than 1 mm in diameter, depth hoar crystals normally exceed 5 mm in diameter approaching the microwave wavelengths. Therefore the depth hoar enhances volume scattering and results in SWE overestimation [*Hall et al.*, 1986]. Since air temperature affects depth hoar formation, *Josberger and Mognard* [2002] incorporated air temperature measurements in the Chang's equation to account for the effect of grain growth on microwave emission. *Grippa et al.* [2004] confirmed that this modification improved accuracy of snow depth estimates for depth hoar dominated snowpack, but the method is applicable only during early winter season when snow grain growth is active.

Besides the physical snowpack properties, the underlying landscape features in the footprint also impact the accuracy of SWE estimates from the passive microwave data. The most notable ones are forest canopy [e.g., *Chang et al.*, 1996; *Dong et al.*, 2005; *Foster et al.*, 2005], water body such as lakes [*Gan et al.*, 2009] and rugged topography [*Foster et al.*, 2005]. The forest canopy tends to mask the microwave emission from snowpack underneath trees [e.g., *Chang et al.*, 1996]. This results in less brightness temperature difference between frequency channels, leading to underestimation of SWE. The amount of underestimation depends on forest density and type of forest and could be as large as 50% [*Foster et al.*, 2005]. The first attempt to correct the forest canopy effect on the SWE estimates was by *Foster et al.* [1997], who added a fractional forest percentage over the pixel to the original Chang's equation as a correction factor. *Goïta et al.* [2003] also developed separate SWE equations for different land cover types (conifer, deciduous, and sparse forest). For complex terrain areas, the sensors viewing angle against the measuring surface differs from one satellite grid cell to another [*Foster et al.*, 2005] and is in reality even heterogeneous within each grid cell due to high terrain irregularities. In addition, in high elevation areas that typically receive more than 100 cm of snow accumulation it is likely that SWE

will be underestimated, given that the penetrating depth of microwave is limited to 50 to 100 cm of snow depth. In contrast to the terrestrial surface, the TBD over lakes tends to diminish due to higher dielectric constant of the water. Due to the large passive microwave footprint (25 km scale), the water body can comprise a significant portion of the pixels in many lake-rich areas such as the northern Hudson Bay area, Canada, Alaska, northern Scandinavia and northern Russia.

Tait [1998] tried to account for the effects of various snowpack characteristics (wet snow, depth hoar), landscape features (evergreen forest, complex terrain) on brightness temperature emission by separating the terrestrial surface over the Northern Hemisphere (mainly Russia and Northern America) into 16 clusters where similar physical snowpack characteristics and terrain features are expected. For each cluster, the best linear multiple regression equation was derived using SWE measurements as a dependent variable and several TBs (19, 37 and 85 GHz frequency channels, both vertical and horizontal polarization) as predictor variables. Among 16 clusters, the largest uncertainty in SWE estimates was observed in complex terrain clusters, especially in the mountains, where 90% confidence intervals on SWE estimates were more than 750 mm wide. *Kelly and Chang* [2003] also attempted to account for the effects of physical snowpack properties and landscape features on the SWE estimates by calibrating the grain size coefficient in the Chang's equation at each satellite grid cell using in-situ measurements available inside each grid cell. Their study covered the Northern Hemisphere, but excluded the mountainous areas in the U.S. due to a concern that the coarse spatial resolution of the passive microwave radiometers (25 x 25 km) is not able to capture high spatial variation in SWE in the mountains. *Tong et al.* [2010] evaluated three different SWE retrieval algorithms (TBD algorithm similar to the Chang's equation, spectral polarization difference algorithm, and nonlinear model - neural artificial network) at three snow stations in the alpine basin in western

Canada. Based on their study, at-site calibration of the ANN model produce most reliable SWE estimates, however, it is extremely difficult to expand the model to the other areas in the basin due to the black-box nature of the model.

1.3.3 Snow modeling

Finally, the snow modeling approach should be mentioned. There are emerging efforts of large scale snow simulations as a part of land surface modeling projects such as North American Land Data Assimilation System (NLDAS) project [*Pan et al.*, 2003] and 30-year retrospective distributed hydrologic simulation over the conterminous U.S.[*Dong et al.*, 2011]. Such continental scale land surface models are capable of producing historical snow variables in a gridded format in a consistent manner. There also exists a large-domain snow modeling at the National Weather Service, National Operational Hydrologic Remote Sensing Center (NOHRSC). For a decade, NOHRSC has successfully executed an energy-based snow model in the Snow Data Assimilation System [*Rutter et al.*, 2009; *Barrett*, 2003] to operationally produce near real time snowpack estimates over the conterminous U.S. at 1-km and 1-hour resolution. However, validations of simulated snowpack variables have not been performed due to lack of independent snow distribution data from observations. Therefore reliability of the snowpack information remains unknown.

1.4 Problem statement and research objectives

1.4.1 Problem statement

This dissertation explored methodologies to map large scale snow distribution over the mountainous areas based on observations (including remote sensing data). The extensive literature reviews of the past studies on the distributions of snowpack variables revealed the following unresolved questions.

Despite accumulated researches on the geostatistical techniques to derive snow distribution from in-situ measurements with promising results, such techniques re-

quire a large number of snow measurements. Therefore, geostatistical approaches are applicable to small areas but are unlikely to be suitable for regional to continental scale snow mapping particularly when one is interested in examining temporal changes in the snow distribution pattern.

Satellite data are attractive for a large-scale snow mapping because of reduced cost and little logistical effort. It also provides the data at a fine temporal interval such as daily. However, the retrieval algorithms have not been evaluated over the complex terrains, and are still assumed to be unreliable for the estimate of mountain snowpack amount.

1.4.2 Research objectives and synopsis

The primary goals of this research are to examine two approaches - 1) statistical approach to interpolate point snow measurements and 2) passive microwave SWE retrieval algorithm, to estimate spatial SWE distributions over the mountainous areas.

This study focused on the multiple mountainous regions of the western U.S. where daily operational snow measurement network is available.

The research began with investigation of spatial and temporal patterns of snowpack variables from climatological perspective based on SNOTEL sites across the whole western U.S. In this analysis, the characteristics of seasonal snowpack density were given more attention due to little research on snowpack density study in terms of large scale spatial variability. The analysis was performed at a point scale, but attempted to provide insight into spatial patterns of snowpack climatology over the western U.S. This research followed up the work by *Serreze et al.* [1999], who analyzed SNOTEL data from 1978 through 1995, but the present study included SD and snowpack density in addition to SWE.

With the same dataset and several auxiliary dataset (climatic wind and physiographic grids), climatological SWE distribution was developed on a monthly basis in

the second part of the research. These climatological estimates are not for immediate application to hydrologic or climate model, but expected to assist in estimating near-real time estimate of SWE distribution. Space and temporal resolution used in this analysis was 4 km and monthly, though the methodology could be applied to any other combinations of the spatial and temporal scales when the desirable scale of the auxiliary data necessary to assist in interpolation is available in the future.

Finally, remote sensing approaches (i.e., microwave data) are examined over the Colorado River basin located in the western U.S. To the best of my knowledge, there have been very few published research studies that investigated the performance of space-borne passive microwave SWE retrievals for the mountainous regions of the western U.S. Therefore the objective was first to evaluate the performances of most commonly used SWE retrieval algorithm for the Colorado River basin and then to investigate if and by how much the accuracy of obtained SWE could be improved through the calibration of the algorithm and a statistical post processing commonly used for the model bias correction. The analyses intended to provide insights into the applicability of the algorithms to spatially and temporally continuous SWE mapping over the basin.

1.4.3 Organization of dissertation

The dissertation consists of three data analytical studies.

The next chapter presents the results of climatological analysis of SNOTEL snow data (SWE, SD and snowpack density) obtained in the mountain regions of the western U.S. These analysis results were published in Journal of Hydrometeorology in December 2008 (Vol. 9, 1416-1426 DOI:10.1175/2008JHM981.1) entitled Spatiotemporal characteristics of snowpack density in the mountainous regions of the western United States.

Chapter 3 discusses the methodology for estimations of SWE distribution over

the entire western United States from the SNOTEL network data. This work was published in Journal of Hydrology in March 2011 (Vol.400, 72-82 DOI:10.1016/ j.jhydrol.2011.01.019) entitled Regional approach for mapping climatological snow water equivalent over the mountainous regions of the western United States.

Chapter 4 presents the analyses and results of the passive microwave SWE retrievals. The results of this analysis were submitted to Hydrological Processes in April 2011 and are currently under peer review.

Chapter 5 provides conclusive remarks and potential future work for each of three studies.

CHAPTER 2

SPATIO-TEMPORAL CHARACTERISTICS OF SEASONAL SNOW PACK PROPERTIES FROM SNOTEL

2.1 Introduction

The goal of this study is to characterize climatic spatio-temporal features of seasonal snow pack characteristics in the mountainous areas of the western United States throughout winter season using daily SWE and SD measurements collected at SNOTEL sites. In particular, this work weighted more on snow pack density to primarily fill in a gap of large scale snow density studies based on the ground measurements. The following section briefly describes the physical seasonal snow pack processes. In Section 2.4, the year-to-year variability as well as the intraannual evolution of snow pack density was examined along with SWE and SD. Section 2.5 characterizes spatial patterns of snow pack densification over the western U.S. Main findings are summarized in Section 2.6.

2.2 Background

Direct ground measurements of SWE are by far sparser than ground measurements of SD. For instance, U.S. and Canadian cooperative stations have provided nearly a million daily SD observations for decades. In contrast, only around 2000 SWE observations at irregular time intervals were available [*Brown et al.*, 2003]. Accurate spatial representation of snow pack density would make it possible to utilize much denser network of ground SD measurements to deduce a better spatial and temporal

representation of SWE through the conversion of SD to SWE given in Eq. 1.1.

Physical snow pack models [e.g., *Jordan*, 1991] that incorporate the snow aging processes represented by snow pack densification and grain growth have often been used to alleviate the lack of sufficient SWE measurements [*Mote et al.*, 2003] needed for many hydrologic applications [e.g., *Thyer et al.*, 2004; *Garen and Marks*, 2005] and climate studies [e.g., *Flanner and Zender*, 2006]. Accurate representation of snow pack density is critical to performance of the snow pack models [*Xue et al.*, 2003]. Typically the snow pack density and its densification rate are modeled using empirical equations with few climate variables used as predictors [e.g., air temperature and precipitation; *Kojima*, 1967; *Brown et al.*, 2003; *Kelly et al.*, 2003]. Due to a very limited availability of snow density measurements, however, spatio-temporal characteristics of snow pack density have not been well understood, particularly at regional or larger spatial scales. Because of this, calibration of model parameters and evaluation of modeled snow density estimates have not been performed.

Density is one of the fundamental properties of snow pack as it directly affects many physical properties of snow [e.g., dielectric, mechanical, and thermal properties; *Langham*, 1981]. Snow pack density is related to snow pack porosity (the fractional volume of air or liquid water portion of snow pack). Typical seasonal snow pack density ranges between approximately 30 and 600 kg/m^3 [*McClung and Schaerer*, 1993]. Based on the density of ice (917 kg/m^3), snow pack density near 30 kg/m^3 implies approximately 97% porosity (3% ice particles and 97% air). This low density is mostly seen for newly fallen snow [*Judson and Doesken*, 2000].

Snow pack densification starts immediately after newly fallen snow reaches the ground. A primary mechanism of densification of seasonal snow pack is continuous compaction derived by overburden pressure that acts on snow grains and sintering process [*Maeno and Ebinuma*, 1983]. The overburden pressure mechanically rear-

ranges snow grains by forcing them together, resulting in reduction of porosity. When snow grains are in contact with each other, necks grow between snow grains through mass transport driven by vapor pressure difference over the convex part (grain) and concave part (neck) of ice surface [*Colbeck*, 1997]. This process is known as sintering and plays a significant role in snow pack densification because it also reduces the porosity of snow pack [*Maeno and Ebinuma*, 1983].

Snow grains by themselves also change in size and shape. This morphological process called snow metamorphism affects the densification process. There are two distinct types of snow metamorphism [*Colbeck*, 1982]: constructive metamorphism (kinetic growth) and destructive metamorphism (equilibrium growth). Constructive metamorphism is grain growth due to recrystallization on existing snow grains and is caused by vapor diffusion resulting from strong temperature gradient within snow pack. A temperature gradient of about 10 °C/m is considered a threshold for the initiation of the constructive metamorphism [*Akitaya*, 1974; *Armstrong*, 1980]. Constructive metamorphism produces large and complex shaped grains called depth hoar. This metamorphism process happens particularly in cold regions such as Alaska [*Hall et al.*, 1986] and the interior of the western United States such as Wyoming during early winter [*Josberger et al.*, 1996]. A snow pack dominated by depth hoar undergoes slower densification than finer grain snow pack because large and complex shaped snow grains hardly experience sintering [*Colbeck*, 1997]. As a result snow pack density stays relatively low throughout the winter season [*Massom et al.*, 2001]. In contrast, when the temperature gradient is weak (warmer air temperature), irregularly shaped snow grains are slowly rounded through mass transfer within snow grains through a process similar to sintering [*Colbeck*, 1982], known as destructive metamorphism. Because rounded grains are more effectively compacted, the density of a snow pack undergoing destructive metamorphism increases steadily [*Kojima*,

1967; *Kaempfer and Schneebeli*, 2007]. Accordingly, higher temperature snow pack increases in density more rapidly. In spring, as the amount of solar radiation increases, net energy inputs into the snow pack become positive and the snow pack temperatures increase. Once the snow pack becomes isothermal at 0 °C, further energy inputs produce snowmelt that begins to fill the snow pack pore space. Once liquid water appears in the snow pack, melt metamorphism becomes the dominant process of the metamorphism [*Anderson*, 1976]. The liquid water causes destructive metamorphism to proceed at a faster rate, and decreases SD while the melt water can be retained within the snow pack. Therefore, snow pack increases in its density more rapidly. Melt metamorphism also involves melt-freeze cycles that happen at the surface the snow pack primarily due to daytime solar radiation. During the melt-freeze cycles, some of the liquid water refreezes during the night, resulting in reduction of snow pack porosity and increase in density.

2.3 SNOTEL data

The analysis used daily SNOTEL data for five months (December through April) from 1999/2000 through 2005/2006 winter season during which the number of sites that provide SD data exceeded 100 sites. Because SNOTEL measurements are fully automated, the daily values were screened for quality check. The quality control procedure on both SWE and SD data described in the Appendix was applied to eliminate erroneous values. In the end, less than 2% of both SD and SWE data were eliminated from all the tests combined.

2.4 Interannual variability in snowpack characteristics

First, we examined how seasonal behaviors of SWE, SD and snow density change from year to year at a given location. For 130 SNOTEL sites for which daily measurements of both SWE and SD were available for the 1999/2000 to 2005/06

period, snow density was computed using Eq. 1.1. Average values of all three variables were calculated for each of the three nonoverlapping 10-day periods per month starting in November and ending in April (the third period in each month may have 8, 9, 10 or 11 days, depending on a month and year). This averaging was performed to reduce effects of random fluctuations on calculated statistics. To examine interannual variability of selected snow characteristics, coefficient of variation (standard deviation normalized by mean and expressed as a percentage) was calculated for each 10-day period for each variable. Figure 2.1 shows coefficients of variation (CV) for SWE, SD and density for midmonth 10-day periods in January, February and March. As can be seen from the figure, there are significant differences in degrees of interannual variability for different snow properties. A significant year-to-year fluctuation is present in SWE data at a majority of the SNOTEL sites. In coastal regions and the southern portion of the western United States, CVs are typically higher than 50% in January. They decrease in February and March to about 30 - 60%. CVs are somewhat lower over the continental region (Montana, Wyoming, and Northern Colorado). At a majority of sites, CVs are about 30 - 40% in January; they decrease to 20 - 30% in March, and increase again in April (not shown in the figure). Similar variability in early spring SWE was found by *Cayan* [1996]. He analyzed SWE measurements at 200 snow courses over 5 decades in the mountain regions in the western United States and reported CVs of April 1 SWE from 20% to over 100%. As can be seen from Figure 2.1, CV estimates for SD are somewhat smaller than corresponding CVs for SWE, but regional patterns are similar for both variables. At the same time, equivalent CV estimates for snow density are significantly lower. At a majority of sites across the western United States, they are less than 20% from midwinter through spring. The low interannual variability of snow pack density was also observed by Brown [2000] who analyzed snow course data collected from 1964 to 1993 over southern Canada.

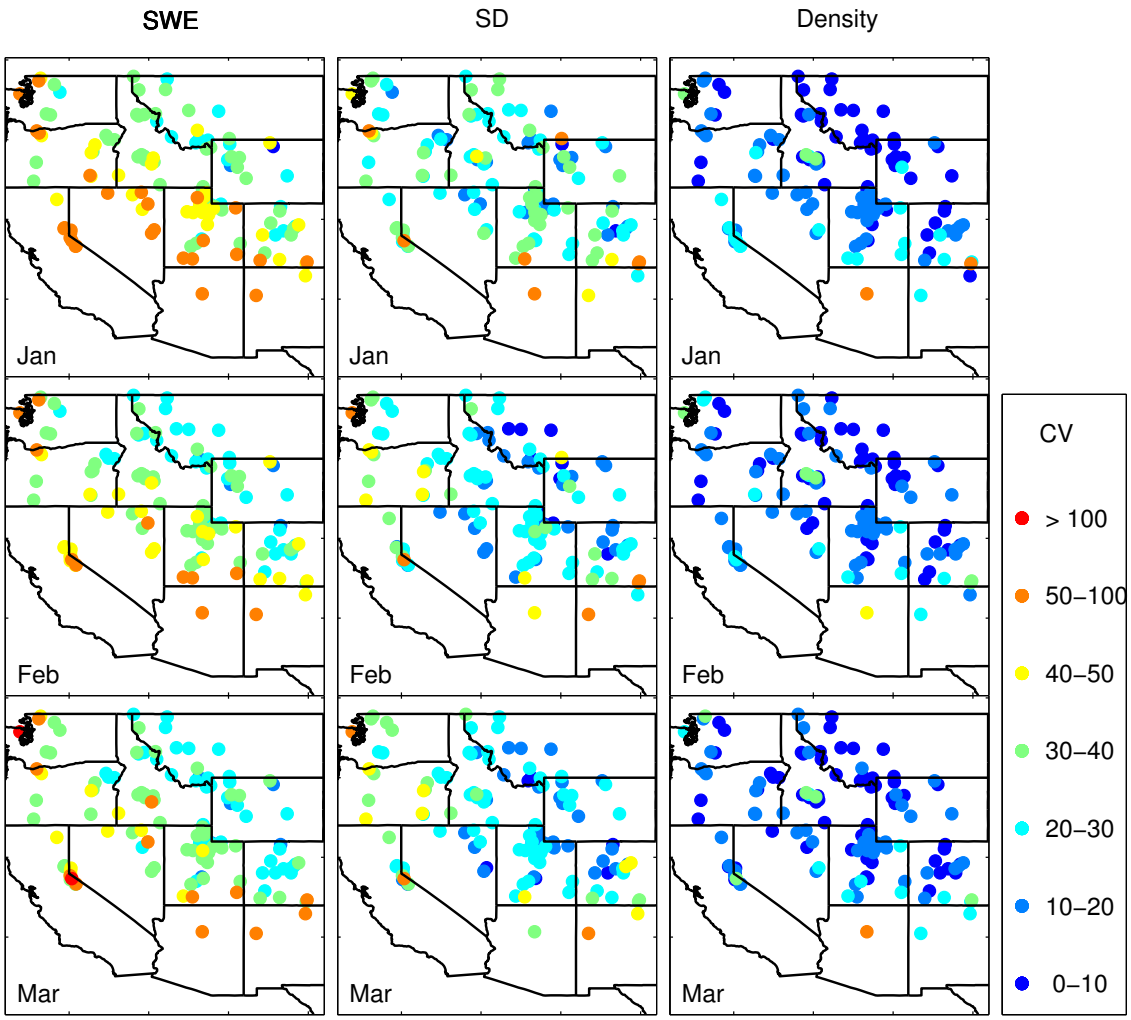

Figure 2.1. Coefficients of variation (in percent) of SWE (left column), SD (middle column) and snow density (right column) for the midmonth 10-day period in January (1st row), February (2nd row) and March (3rd row).

In order to further examine year-to-year variability of the three snow pack characteristics, the following three SNOTEL sites were selected for detailed analysis: Park Creek Ridge in Washington (48.45 N, 120.92 W, 1403 m.a.s.l), Bloody Dick in Montana (45.17 N, 113.50 W, 2303 m.a.s.l), and Kings Cabin in Utah (40.72 N, 109.55 W, 2662 m.a.s.l). The sites were chosen primarily because snow courses collocated at those sites provided long-term SWE and SD measurements. The snow course data extends back to 1928 at Park Creek Ridge, to 1948 at Bloody Dick, and to 1930 at Kings Cabin. In addition, selected sites are located in different geographical regions and at different elevations.

The difficulty with the snow course data is that measurements are typically made on a single day at the end of each month (mostly from January through April), and not always at the same date. Also, there are months or even years when no measurements were taken. For this analysis, snow course measurements of SWE and SD taken at the end of each month (from January through April) were combined with the corresponding SNOTEL measurements on the 25th of each month. Table 2.1 shows CV estimates for all three snow variables calculated from combined records and, and for comparison, CV estimates for all three variables calculated from only 7-year long SNOTEL record. As can be seen from Table 2.1, CV estimates for snow density are similar for both records; they are less than 15% at Park Creek Ridge and Bloody Dick sites and around 20% at Kings Cabin. CVs are significantly higher for SWE and SD for both datasets. To examine intraseasonal and interannual variations in daily snow data, daily time series were plotted for all three snow variables for 7 winter seasons (Figure 2.2). Similar to the previous analysis of 10-day averaged data, the analysis of daily data showed that there is a considerable inter-annual variability in SWE and SD, but significantly less year-to-year variation in snow density. It also becomes visible that densification trends are generally linear for all three sites.

Table 2.1. Coefficients of variation (in percent) for daily estimates of SWE, SD and density computed at selected sites. For each site, the first row shows CVs estimated using both SNOTEL measurements taken on the 25th of each month and historical snow course data from January to April; second row (in parenthesis) shows corresponding CVs estimated from 7-years of SNOTEL data.

		Coefficients of variation (%)		
	Month	Park Creek Ridge	Bloody Dick	Kings Cabin
SWE	Jan	35(37)	36 (36)	58(61)
	Feb	32(38)	30(36)	39(41)
	Mar	31(42)	27(34)	34(38)
	Apr	46(48)	48(42)	55(66)
SD	Jan	38(46)	32(20)	37(40)
	Feb	29(45)	21(26)	30(24)
	Mar	30(51)	23(30)	32(40)
	Apr	41(48)	51(37)	54(65)
Density	Jan	15(13)	9(9)	24(24)
	Feb	11(9)	15(12)	17(24)
	Mar	10(6)	12(16)	19(18)
	Apr	8(5)	17(22)	23(15)

However, at the Kings Cabin and Bloody Dick sites, densification rates change around the beginning of March. About the same time, and before the SWE peaks, SD starts decreasing. The change in densification change could be result of abrupt snow pack compaction possibly due to appearance of liquid water inside the pack, which enhances destructive snow metamorphism.

2.5 Spatial patterns of snowpack density and densification

Based on the results from the previous section, density magnitudes may have little year-to-year variations, but they appear to be location dependent. This finding prompted us to further investigate whether: a) densification trends from Figure 2.2 are typical for the entire western United States, and b) whether similar snow pack densities and densification rates occur in spatially coherent manners. Cluster analysis was used to obtain qualitative information on spatial patterns.

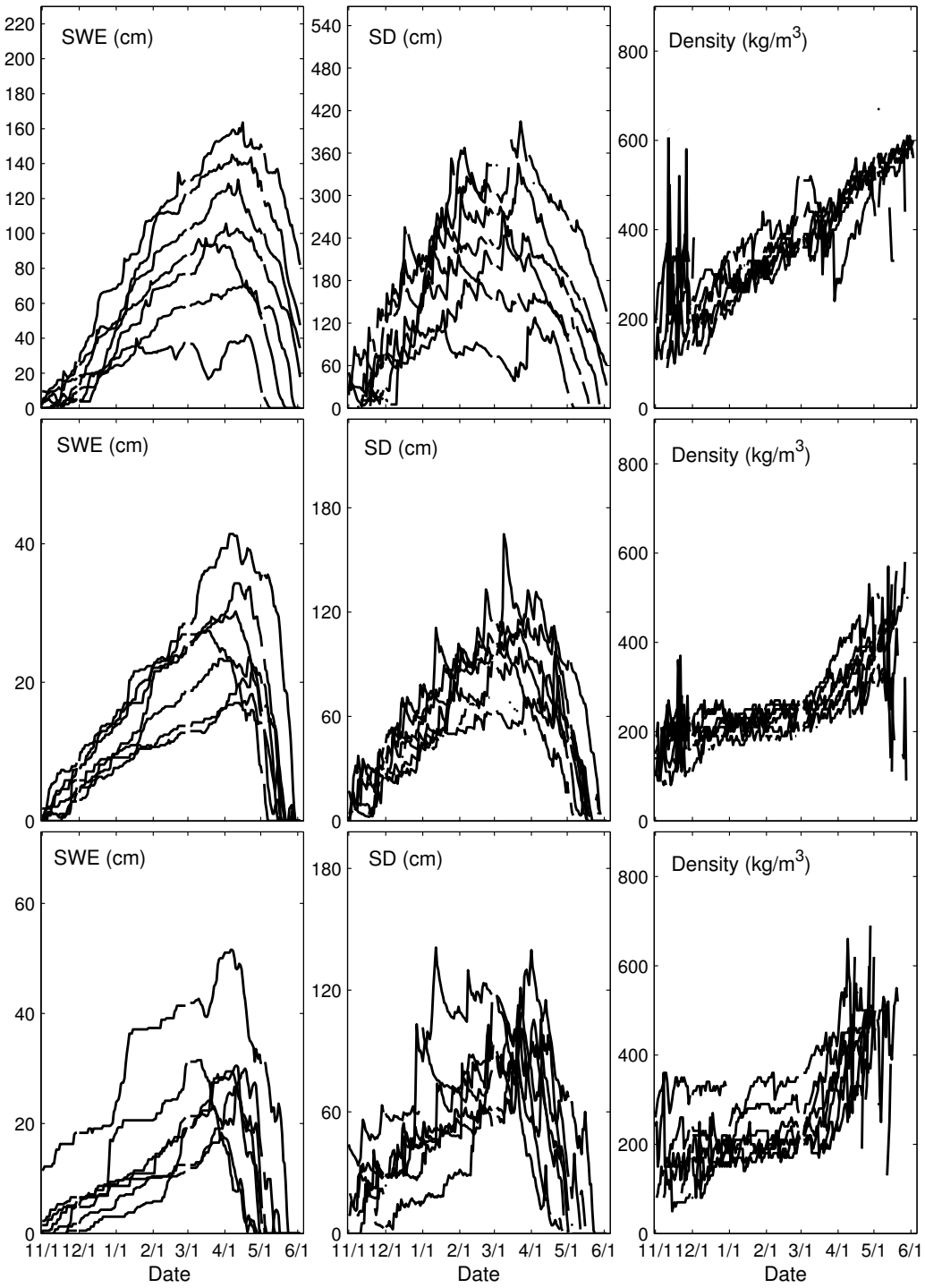

Figure 2.2. Daily time series of SWE (column 1) , SD (column 2) and snowpack density (column 3) from November 1 to May 30 for 7 winter seasons starting in 1999/2000 at three selected SNOTEL sites. Each row corresponds to one site: Park Creek Ridge, Washington; Kings Cabin, Utah; Bloody Dick, Montana from top to bottom.

In cluster analysis, the similarity between sites is measured by the Euclidian distance in terms of the selected attribute variables *Everitt et al.* [2001]. The equation for Euclidian distance ($d_{i,j}$) between site i and site j is given by the following expression:

$$d_{i,j} = [\sum_{k=1}^{K}(x_{i,j} - x_{j,k})^2]^{1/2} \tag{2.1}$$

where $x_{i,k}$ is the k-th ($k = 1, \cdots, K$) attribute variable at site i, and $x_{j,k}$ is k-th attribute variable at site j. When the attribute variables consist of the time series of a single type of variable, Eq. 2.1 can be decomposed into three components: difference in seasonal means of time series at site i and site j ($\overline{x_i}$ and $\overline{x_j}$), difference in seasonal variability (S_i and S_j), and linear correlation (r_{ij}) between two time series:

$$d_{i,j} = c[(\overline{x_i} - \overline{x_j})^2 + (S_i - S_j)^2 + 2S_iS_j(1 - r_{ij})]^{1/2} \tag{2.2}$$

where c is a constant. This concept was introduced by *Fovell* [1997], who delineated homogeneous climate zones over the contiguous United States by applying this type of clustering strategy with time series data of air temperature and precipitation independently and then intersecting two cluster maps.

Using the time series of a single variable provides two important advantages for cluster analysis [*Fovell*, 1997]. First, because all attributes have the same measurement unit, standardization that is usually performed to assign equal weights to all the attribute variables is unnecessary. The second advantage is related to data redundancy. Like other types of multivariate statistical analyzes (such as multiple regression analysis), redundancy of attribute variables might have negative effects on cluster analysis results [*Fovell and Fovell*, 1993]. If correlated attribute variables are used for Euclidian distance computation, they dominate other attributes; therefore, they have more influence on the clustering outcome. In contrast, inclusion of long term continuous time series of a single variable at finer time step may have positive effects on the results. This is because the statistics (mean, standard deviation, and

correlation coefficient) used in the Eq. 2.2 are likely to gain a confidence owing to increased samples.

In this study, 10-day average climatological density values (based on 2000/01 through 2005/06 years) from December through April calculated at 181 SNOTEL sites were used for cluster analysis. Therefore, 15 attribute variables (three 10-day average values per month times 5 months) were used to evaluate the similarity between SNOTEL sites.

There are two types of clustering algorithms: hierarchical and nonhierarchical. The hierarchical clustering algorithms perform a series of either successive partitioning (agglomerative method) or successive merging (division method). The agglomerative method starts with n clusters containing a single membership and then continues aggregating two clusters until a single cluster containing all the n memberships is obtained. Division method runs in the opposite way, splitting one cluster into two until all the n memberships are separated into n clusters. In contrast to the hierarchical method, the nonhierarchical algorithm permits objects to change group membership through the cluster formation process. The partitioning method usually begins with an initial solution, after which reallocation occurs according to some optimality criterion. There have been some discussions on what type of clustering approach is appropriate for analyzing meteorological data [e.g., *Kalkstein et al.*, 1987; *Fovell and Fovell*, 1993]. In this study, we chose one of the nonhierarchical clustering methods, K-mean algorithm, because of its resistance to outliers [*MacQueen*, 1967]. We also tried one of the hierarchical clustering algorithms, the Wards method, but it produced almost identical clusters to the K-mean algorithm results.

We also investigated the influence of different groupings of clusters on the spatial contiguity of SNOTEL sites. SNOTEL sites were first divided into two clusters. A map of the western United States with sites assigned to each of the two clusters is

shown in the top left panel of Figure 2.3. Time series of mean snow pack density for each cluster are shown to the right of the spatial map. As can be seen from the top-left panel of Figure 2.3, high and low density regimes are clearly separated for the 2-cluster case. Cluster 1 includes mostly sites located in the coastal region and cluster 2 consists of sites in the continental region. That suggests that the most significant factor that separates different snow density regimes is proximity to a large water body (in this case, the Pacific Ocean).

For the 3-cluster case (Figure 2.3 middle panels), many sites assigned to new cluster (cluster 3) are located between coastal region (cluster 1) and continental region (cluster 2). This longitudinal transition from higher density snow pack to lower density is still present, but clusters 2 and 3 seem to be spatially disconnected. However, when some mountain ranges are looked into, regional patterns become apparent. For instance, cluster 2 contains sites on the west side and cluster 3 contains sites on the eastern side of the Colorado Rocky Mountains. Sites in Utah are assigned to cluster 3 except for sites in the Uinta Mountains and the southern portion of the Wasatch Mountains.

We further partitioned the SNOTEL sites into four clusters (Figure 2.3, bottom panels). Several sites located in the continental area that were assigned to cluster 3 in previous analysis (3-cluster case) were reassigned to the cluster 2, making the spatial patterns more contiguous than in the 3-cluster case. The new cluster (cluster 4) is composed of sites with the lowest density throughout winter, but is spatially discontinuous. It appears that the majority of sites assigned to the cluster 4 are located at the highest elevations in the continental western United States, such as the Uinta Mountains in Utah and the central Colorado Rocky Mountains. Increasing the number of clusters to five or more (not shown in the figure) did not lead to detection of significantly different density regimes.

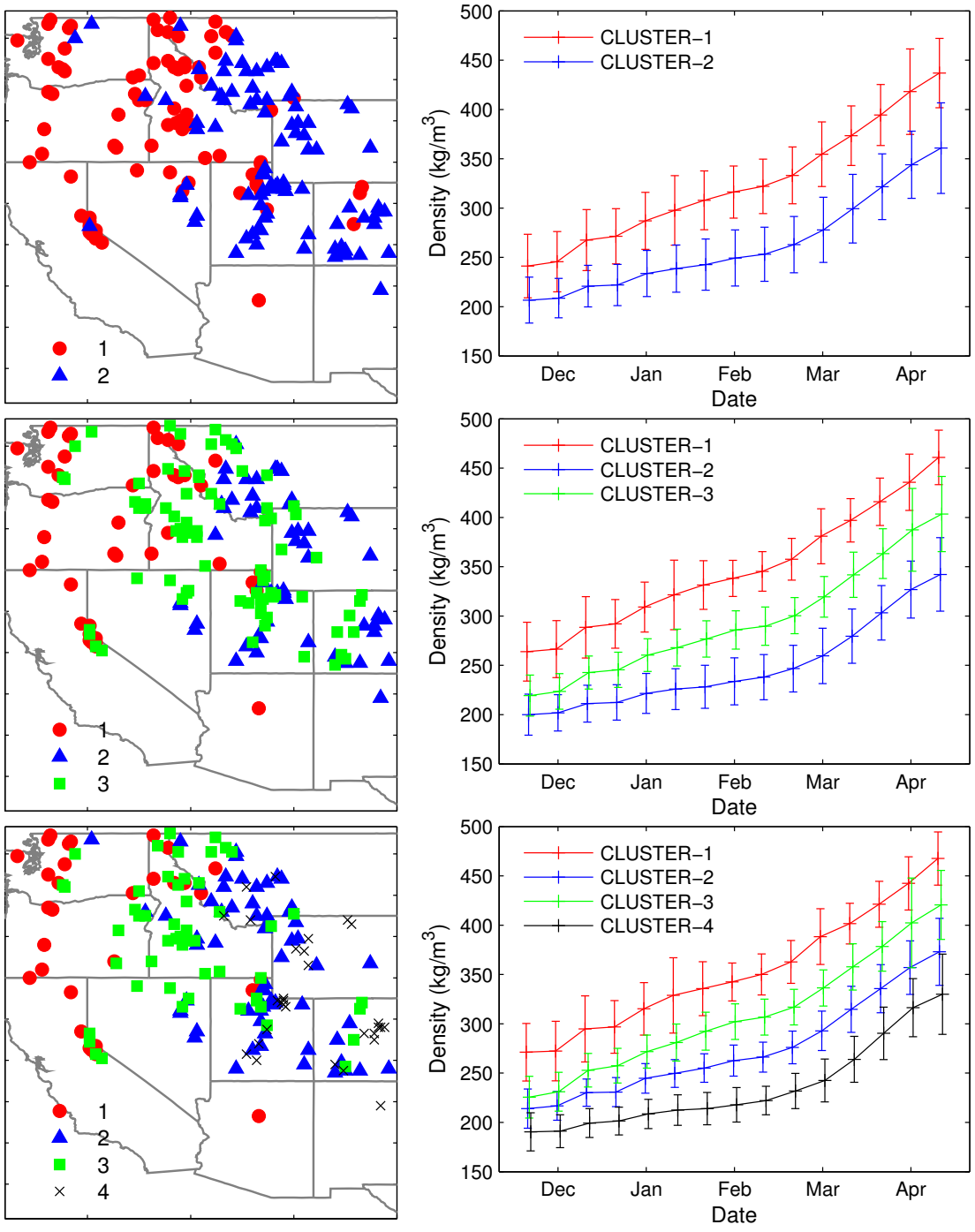

Figure 2.3. Left panels show a map of the western United States with SNOTEL sites assigned to different clusters for two-, three-, and four-cluster cases (from top to bottom). Right panels show corresponding time series of average snow density for each cluster. Error bars in the time series indicate mean values plus and minus one standard deviations.

Inspection of time series of mean density for different clusters (right panels in Figure 2.3) pointed to an interesting link between snow pack densification rates and snow density magnitudes. The higher the seasonal mean density is, the faster the midwinter densification rate. This characteristic can be seen in all the cluster cases. Also, as can be seen from Figure 2.3, early-March snow pack densifies at similar densification rate for all clusters at a rate that is faster than any midwinter densification rate.

We used a linear regression approach to quantify densification rates for each of four clusters. Time series were separated in two periods: midwinter (from December 1 through March 1) and early spring (March 1 through April 31). As can be seen from Table 2.2, densification rates (slope terms in regression equations) for midwinter snow pack vary in space implying snow pack densification is affected by regional climate when snow pack is cold and likely to be dry. However, densification rates for spring snow pack are 2.0 kg/m^{3}per day with very little spatial variability.

To examine what factors might control these spatial patterns, box-plots of selected terrain characteristics were constructed for each cluster in the 4-cluster case (Figure 2.4). Selected characteristics were latitude, longitude, elevation (in meters), eastness (sine of azimuthal angle), northness (cosine of azimuthal angle), and slope inclination. Latitude, longitude and elevation are at-site characteristics from SNOTEL locations. Other selected terrain variables (eastness, northness, slope) were derived from 1-km Digital Elevation Model (DEM) dataset. Chosen terrain variables control local meteorological conditions such as air temperature and solar energy flux, and were investigated as possible predictors of snow characteristics in earlier snow studies [e.g., *Balk and Elder*, 2000; *Erxleben et al.*, 2002; *Fassnacht et al.*, 2003; *Erickson et al.*, 2005]. Many studies have also reported that the new fallen snow is denser in warmer

Table 2.2. Regression equations for midwinter (December 1 through March 1) and early spring (March 1 through April 31) snowpack densification per each cluster. Clusters are ordered in west-east direction. ρ_s is snow density in kg/m^3 and t is time in days.

	December 1 - March 1	March 1 - April 31
Cluster 1	$\rho_s = 269.7 + 1.1t$	$\rho_s = 363.6 + 2.0t$
Cluster 2	$\rho_s = 227.1 + 1.0t$	$\rho_s = 316.1 + 2.1t$
Cluster 3	$\rho_s = 213.4 + 0.7t$	$\rho_s = 275.0 + 2.0t$
Cluster 4	$\rho_s = 189.1 + 0.4t$	$\rho_s = 226.4 + 2.1t$

environments [*LaChapelle*, 1962; *Grant and Rhea*, 1974; *McGurk et al.*, 1988; *Judson and Doesken*, 2000]. As can be seen from Figure 2.4, longitude and elevation most effectively discriminate between densification regimes. In the western United States, longitude is correlated to the proximity to the Pacific Ocean. The coastal region of the western United States is characterized by the abundant precipitation and relatively high air temperatures [*Serreze et al.*, 1999], which are contributors to high snow pack density throughout winter.

2.6 Summary

Spatio-temporal characteristics of seasonal snow pack density were examined throughout the winter season based on 7 years of daily snow pack observations (1999/2000 to 2005/06) at SNOTEL sites over the western United States.

In contrast to SWE and SD, snow pack density exhibits rather small year-to-year variability throughout the winter season at most SNOTEL sites. This low inter-annual variability of snow density is beneficial for several applications. To start with, climatological values of snow pack density at any location of interest could be estimated with confidence after only several years of SWE and SD measurements become available. Also, climatological values of snow pack density could be used

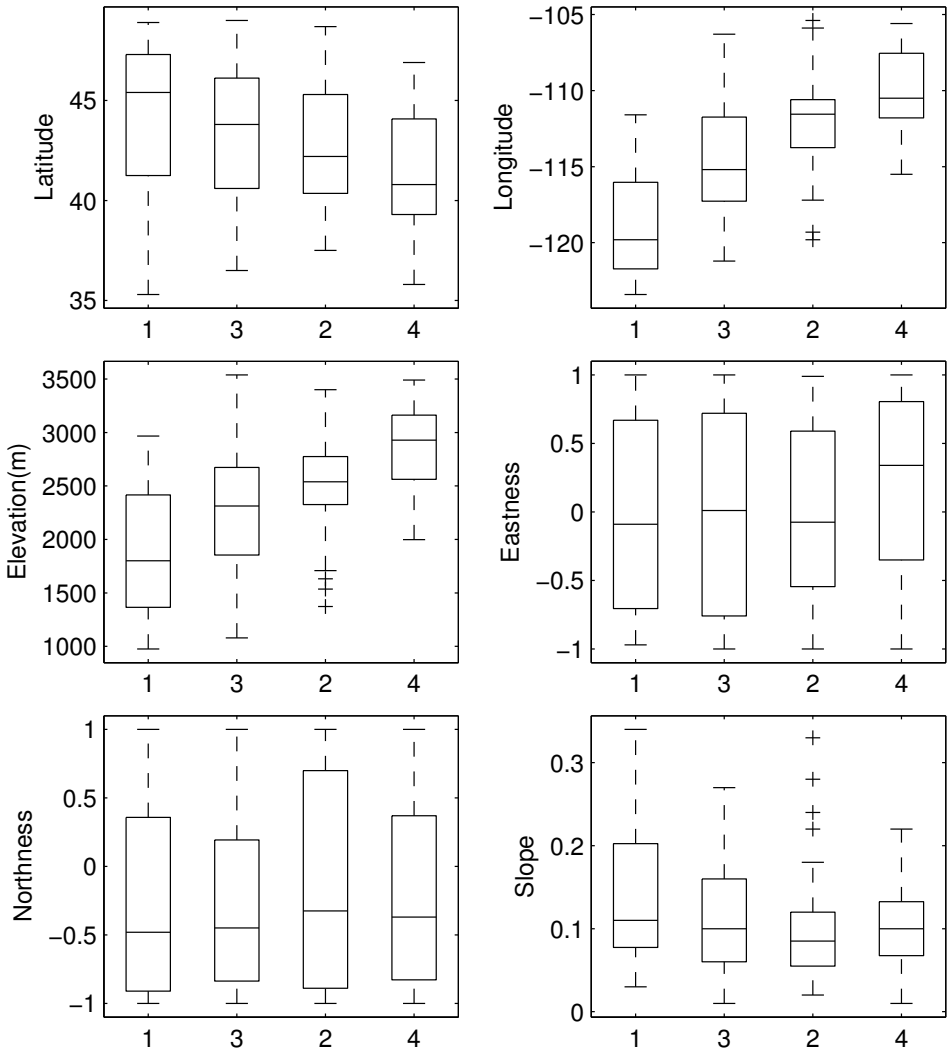

Figure 2.4. Box plot of six selected terrain characteristics for each of four clusters. A box height indicates the interquartile range, and a whisker extends 1.5 times the interquartile range.

with SD measurements to estimate real-time SWE data needed for many hydrologic applications. This could be very useful, for example, in lower elevation areas in the western United States where only SD data are available from the National Weather Service (NWS) Cooperative Observer stations and NWS First Order stations.

Also, historical SD measurement and developed snow pack density climatological maps could be used to obtain historical SWE data and to create climatological SWE maps. They are useful for climate studies as they provide information on longer-term fluctuations of snow pack amounts associated with climate fluctuations [*Mote et al.*, 2005]. The SWE climatology could also be useful for calibration of hydrologic models that include a snow component and for calibration of empirical equations used to estimate SWE from remote sensing data such as passive microwave data.

In order to characterize complexity of spatial and temporal variability of snow pack density, we used cluster analysis. Cluster analysis revealed four distinct regions, each having different density magnitude and densification throughout winter months. Patterns of snow pack densification from each cluster were characterized as follows. During early and midwinter, densification rate is correlated with density. The higher the magnitude of density is, the faster the densification is. Around the beginning of March, however, snow pack densification becomes faster but relatively constant (2.0 kg/m^3 per day) regardless of location. It was also found that longitude (representing the proximity of the Pacific Ocean) and elevation are important variables that discriminate between different snow pack density regimes.

Although there are more than 700 SNOTEL sites across the western U.S., at the moment only 130 sites had sufficiently long records to be useful for this study. As the number of SNOTEL sites increases every year and additional SD sensors are installed at existing sites, more detailed analysis of spatio-temporal characteristics of mountain snow pack density will be feasible in a few years.

CHAPTER 3

REGIONAL APPROACH FOR MAPPING CLIMATOLOGICAL SWE OVER THE MOUNTAIN REGIONS OF THE WESTERN U.S.

3.1 Introduction

The study presented in this chapter intended to follow up on the large-scale (e.g., continental scale) SWE interpolation studies descried in the Chapter 1 [i.e., *Fassnacht et al.*, 2003]. This study investigated the ability of simple regional regression-based approaches to map SWE climatology over the mountainous regions of the western United States.

The rest of the chapter is structured as follows. All datasets used in the study are briefly described in Section 3.2. The development of the regional equations is described in Sections 3.3 and 3.4. First, in Section 3.3, regions with homogenous climate and similar snow pack processes are delineated for the entire western U.S. Then, monthly SWE climatological grids are estimated for October-April period through regionally calibrated equations in Section 3.4. Estimation errors are evaluated through jack-knife method. Finally, the main findings of the study and potential applications for this product are discussed in Section 3.5.

3.2 Datasets

3.2.1 In-situ SWE measurements

In-situ SWE measurements at the SNOTEL across the western United States from October 1980 through April 2004 were used for this analysis. The quality control (see

Appendix) left complete daily SWE dataset at 403 SNOTEL sites shown in Figure 3.1.

3.2.2 Precipitation and air temperature grids

Monthly total precipitation and average daily air temperature values at a 2.5-arc-minute (approximately 4-km) resolution for each month for the 1980-2004 period were obtained from the PRISM (Parameter-elevation Regressions on Independent Slopes Model) Climate Groups database (http://www.prismclimate.org). Detailed descriptions of the PRISM products and the techniques used to develop those products can be found in several publications [e.g., *Daly et al.*, 1994, 2008]. In short, the PRISM climate mapping system incorporates point measurements of precipitation, temperature, and other climatic variables together with a digital elevation model and expert knowledge of complex topographic effects on climatic variables to produce monthly gridded estimates of several meteorological variables over the conterminous U.S.

3.2.3 Elevation grids

One-arc-sec (approximately 30-m) digital elevation model (DEM) data were obtained from the National Elevation Dataset through the U.S. Geological Surveys National Map Seamless Server (http://seamless.usgs.gov). Elevation grids were used for two purposes: they were included in a set of potential predictors of climatological SWE (in Section 3.4), and were used to estimate daily clear sky solar radiation that was in turn used as an attribute variable for cluster analysis (see below and Section 3.2.4).

3.2.4 Solar radiation grids

Daily total direct solar beam (J/m^2) was estimated from a model that uses geometric relationship between astronomical solar position and latitude and local terrain properties (such as orientation, incline and local topographic shadowing)

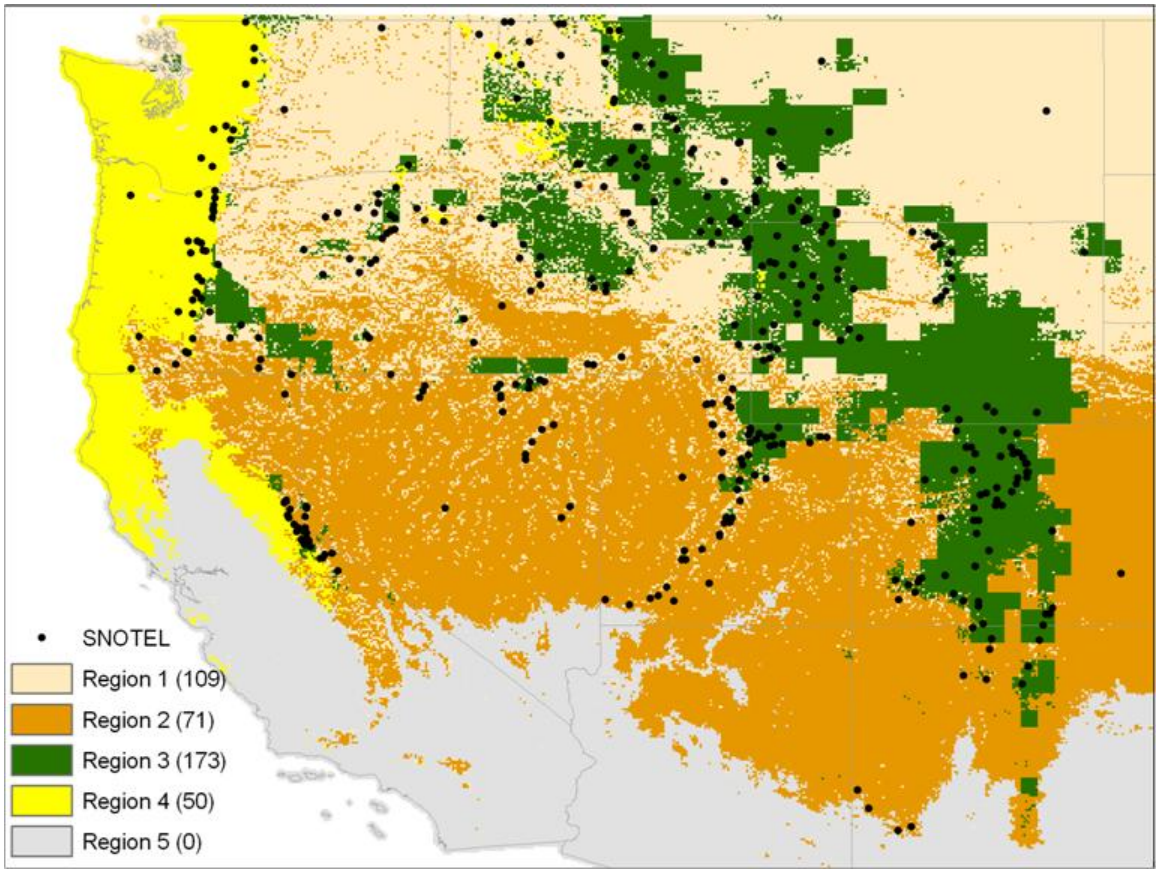

Figure 3.1. Five snow climate regions for the western United States delineated through cluster analysis. Region 3 is characterized by wind speed data that were available at lower resolution (32-km vs. 4-km for other variables). Numbers in parentheses in the legend indicate number of SNOTEL sites used in this study in each region.

computed from the DEM data [*Dozier and Frew*, 1990; *Kumar et al.*, 1997; *Šúri and Hofierka*, 2004]. Daily total direct solar beam was computed for each 1-arc-sec grid cell on the 15th of each month from October to April, and an assumption was made that the computed direct radiation represents direct radiation value for each month. The computation used a clear sky condition. Therefore the scattering effect of atmospheric aerosols and clouds was not taken into account.

3.2.5 Wind speed grids

Wind speed data were obtained from the National Centers for Environmental Predictions (NCEP) North American Regional Reanalysis (NARR) dataset [*Mesinger et al.*, 2006]. The NARR is a hydrometeorological dataset over North America derived using the 32-km resolution. NCEPs Eta model together with the Regional Data Assimilation System (RDAS) which assimilates various types of satellite, radar and surface observations. The 3-hour near-surface wind speed estimates are available over the North American domain from 1979. Brief discussions on the derivation and accuracy of NARRs wind speed data can be found in *Mesinger et al.* [2006].

3.3 Delineation of homogeneous snow climate regions

Regionalization based on similar hydrologic processes is typically a first step for modeling and prediction for ungauged basins since the analyses of regionally grouped data can reveal specific regional relationships that could lead to unbiased estimations. With this in mind, the development of regional regression-based equations for the estimation of monthly climatological SWE grids starts with a delineation of homogeneous regions in terms of the seasonal snow pack accumulation and ablation processes. However, the identification of homogeneous regions requires a considerable amount of subjective judgments.

A few snow studies presented some kind of regionalization for the snow pack

climate. For example, *Serreze et al.* [1999] and *Hatch* [2006] used geographical regionalization scheme based on major mountain regions in the western United States. *Sturm et al.* [1995] created a 0.5-degree mesh over the North America and Eurasia and classified each grid cell into one of the six seasonal snow pack climate regions (hereafter Sturms snow classification). The snow climate regions were delineated by relating the physical properties of snow pack (crystal morphology, depth, wetness, density, and thermal conductivity) to average precipitation, air temperature and wind speed characteristics. Lacking global gridded wind speed data, a vegetation type was used as a proxy for wind speed; tall vegetation was equated with low wind speed, and short vegetation with high wind speed. *Fassnacht and Derry* [2010] classified SNOTEL sites within the upper Colorado River Basin into the regions of similar snow accumulation and ablation patterns using a self-organizing map approach, but this type of regionalization approach requires an additional classification of ungauged locations to one of the delineated regions to generate spatially continuous classification maps. *Farmer et al.* [2010] utilized hierarchical clustering algorithm and gridded passive microwave brightness temperature data (25 km resolution), which contains information on snow accumulation and melt processes, to classify the Canadian prairie area into 18 homogeneous snowpack regions.

For this study, a spatially contiguous classification method similar to Sturms and Farmers classification is essential to estimation of SWE climatology at ungauged locations. Cluster analysis with the gridded attribute data was used to delineate homogeneous snow climate regions for the western United States by assigning every 4-km grid cell to one of the regions. Various meteorological and geographic variables that directly or indirectly affect snow accumulation and ablation were considered as potential attribute variables for the cluster analysis. Precipitation, air temperature, solar radiation and wind speed were selected among the meteorological variables

since they are major drivers of snow pack mass and energy exchange processes [e.g., *Marks and Dozier*, 1992], thus directly affecting snow accumulation and ablation. Latitude, longitude and elevation were selected as representative geographic variables that influence spatial variability of the meteorological variables and thus indirectly affect snow accumulation and ablation processes. For the meteorological variables, both, the magnitude and temporal evolution were considered in the regionalization. All meteorological variables were averaged over the 1980-2004 period. The spatial and temporal resolution for the analysis was selected to match the resolution of the precipitation and temperature data obtained from the PRISM database (approximately 4-km spatial resolution and 1-month temporal resolution). The geographic and solar radiation grids were aggregated into 4-km grid. The NARRs wind speed estimates, available at 32-km resolution, were assumed to be uniform across all 4-km cells inside a corresponding 32-km cell. Average monthly wind-speed estimates were obtained from corresponding 3-hour estimates.

Regionalization based on similar hydrologic processes is typically a first step for modeling and prediction for ungauged basins since the analyses of regionally grouped data can reveal specific regional relationships that could lead to unbiased estimations. With this in mind, the development of regional regression-based equations for the estimation of monthly climatological SWE grids starts with a delineation of homogeneous regions in terms of the seasonal snow pack accumulation and ablation processes. However, the identification of homogeneous regions requires a considerable amount of subjective judgments.

A few snow studies presented some kind of regionalization for the snow pack climate. For example, *Serreze et al.* [1999] and *Hatch* [2006] used geographical regionalization scheme based on major mountain regions in the western United States. *Sturm et al.* [1995] created a 0.5-degree mesh over North America and Eurasia and

classified each grid cell into one of the six seasonal snow pack climate regions (hereafter Sturms snow classification). The snow climate regions were delineated by relating the physical properties of snow pack (crystal morphology, depth, wetness, density, and thermal conductivity) to average precipitation, air temperature and wind speed characteristics. Lacking global gridded wind speed data, a vegetation type was used as a proxy for wind speed; tall vegetation was equated with low wind speed, and short vegetation with high wind speed. *Fassnacht and Derry* [2010] classified SNOTEL sites within the upper Colorado River Basin into the regions of similar snow accumulation and ablation patterns using a self-organizing map approach, but this type of regionalization approach requires an additional classification of ungauged locations to one of the delineated regions to generate spatially continuous classification maps. *Farmer et al.* [2010] utilized hierarchical clustering algorithm and gridded passive microwave brightness temperature data (25 km resolution), which contains information on snow accumulation and melt processes, to classify the Canadian prairie area into 18 homogeneous snowpack regions.

For this study, a spatially contiguous classification method similar to Sturms and Farmers classification is essential to estimation of SWE climatology at ungauged locations. Cluster analysis with the gridded attribute data was used to delineate homogeneous snow climate regions for the western United States by assigning every 4-km grid cell to one of the regions. Various meteorological and geographic variables that directly or indirectly affect snow accumulation and ablation were considered as potential attribute variables for the cluster analysis. Precipitation, air temperature, solar radiation and wind speed were selected among the meteorological variables since they are major drivers of snow pack mass and energy exchange processes [e.g., *Marks and Dozier*, 1992], thus directly affecting snow accumulation and ablation. Latitude, longitude and elevation were selected as representative geographic variables

that influence spatial variability of the meteorological variables and thus indirectly affect snow accumulation and ablation processes. For the meteorological variables, both the magnitude and temporal evolution were considered in the regionalization. All meteorological variables were averaged over the 1980-2004 period. The spatial and temporal resolution for the analysis was selected to match the resolution of the precipitation and temperature data obtained from the PRISM database (approximately 4-km spatial resolution and one-month temporal resolution). The geographic and solar radiation grids were aggregated into 4-km grid. The NARRs wind speed estimates, available at 32-km resolution, were assumed to be uniform across all 4-km cells inside a corresponding 32-km cell. Average monthly wind-speed estimates were obtained from corresponding 3-hour estimates.

Similar to other types of multivariate statistical analyses, inclusion of highly correlated attribute variables is not desirable in cluster analysis, as redundant attribute variables could dominate clustering outcomes [e.g., *Fovell and Fovell*, 1993]. Cross-correlation analysis for the selected geographic variables and meteorological variables averaged for the winter season was performed and the results are shown in Table 3.1. As can be seen from the table, all the geographic variables are correlated with at least one meteorological variable. For example, latitude is highly correlated with solar radiation and air temperature (correlation coefficient R = -0.81 and -0.68, respectively); longitude is correlated with precipitation (R = -0.54), and elevation is correlated with air temperature (R = -0.60). Because of the more direct relationship between SWE and meteorological variables than geographic variables, only meteorological variables were considered for the cluster analysis.

Inclusion of attribute variables with different units and ranges of the magnitudes is also undesirable for the cluster analysis. Therefore, all the attribute variables were standardized as follows:

Table 3.1. Cross-correlation coefficients (R) for various geographic and meteorological variables (averaged over October-April, 1980-2004 period) considered as potential attribute variables for cluster analysis. $|R| > 0.5$ is shown in bold.

	Latitude	Longitude	Elevation	Precipitation	Temperature	Wind speed	Solar radiation
Latitude	1.00						
Longitude	-0.16	1.00					
Elevation	-0.12	0.39	1.00				
Precipitation	0.26	**-0.54**	-0.14	1.00			
Temperature	**-0.68**	-0.29	**-0.60**	-0.01	1.00		
Wind speed	0.22	0.16	0.33	0.16	-0.38	1.00	
Solar radiation	**-0.81**	0.17	0.14	-0.25	0.46	-0.18	1.00

$$z_{i,j} = (x_{i,j} - \overline{x_j})/S_j \tag{3.1}$$

where $x_{i,j}$ and $z_{i,j}$ are the j-th ($j = 1, \cdots, J$) original and standardized attribute variables at grid cell i, respectively, and $\overline{x_i}$ and s_j are the mean and standard deviation of the j-th attribute variable over the whole domain (i.e., the entire western United States), respectively.

K-mean is one of many clustering algorithms that could be used to statistically partition n objects (in this case, 248,050 grid cells). The K-mean algorithm was selected over the hierarchical clustering algorithms here, because it it is computationally more efficient and also more resistant to outliers in the attribute variables [*MacQueen*, 1967].

The K-mean algorithm iteratively assigns objects to a prespecified number of clusters (K) through the following procedure. First, initial centroids for all clusters (i.e., mean values of each attribute variable over a cluster) are obtained from a random partition of n objects into K clusters. Then, each object is assigned to the cluster with the nearest centroid according to similarity of the attribute variables considered,

which is measured by the Euclidian distance [*Everitt et al.*, 2001]. After all the objects have been reassigned and the centroids are updated for each cluster, they are used as new seed centroids for the next iteration. At the same time, the within-cluster sum of the squared Euclidian distances between each object and the centroid of its currently assigned cluster (F) is computed as a follows:

$$F = \sum_{k=1}^{K} \sum_{i=1}^{n_k} \sum_{j=1}^{J} (z_{i,j} - \overline{x}_{k,j})^2 \tag{3.2}$$

where $z_{i,j}$ is a j-th standardized attribute variable of object i, is the mean of j-th standardized attribute variable within k-th cluster, and n_k is the number of objects within the k-th cluster. Iteration terminates when the centroids of all clusters do not change, that is, when F is minimized.

Determining an optimal number of clusters is one of the subjective aspects of many clustering techniques, including K-mean. Rather than relying on some of the indices commonly used for determination of the final number of clusters (e.g., the silhouette validation, Dunns Validity Index, Goodman-Kruskal index, or C-index), the optimal number of the clusters was determined by examination of change in selected statistical performance measures of the regional regression equations developed in the next section with the increase in number of clusters. Root mean squared error (RMSE) and correlation coefficient (R) statistics were used to measure the performance of the regional regression equations for a varying number of the regions. In the next section, 2-, 5-, and 10- region cases will be examined in more detail. As will be shown in the next section, five regions for the western United States seem to be sufficient for the estimations of monthly SWE climatology throughout the analysis period except in April.

Figure 3.1 shows the spatial distribution of five snow climate regions delineated through the cluster analysis. The regions match fairly well with the Sturm snow classification shown in Figure 3.2 (except that their ephemeral region is now split

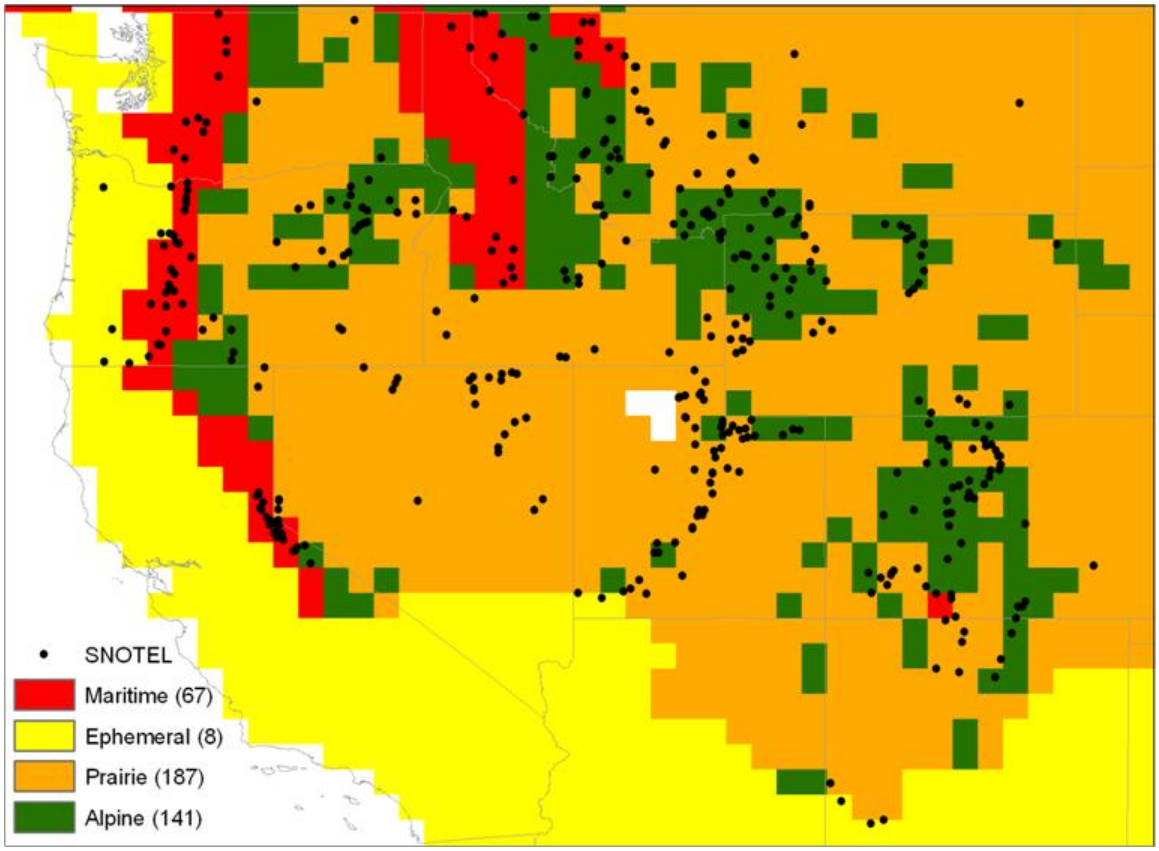

Figure 3.2. Snow climate regions in the western United States delineated by *Sturm et al.* [1995]. Grid cells over large water bodies were not classified. Black dots indicate locations of current SNOTEL sites. Numbers in parentheses in the legend indicate number of SNOTEL sites used in this study in each region.

into two regions - regions 4 and 5). This is probably because both studies considered similar meteorological characteristics for the regional delineations, although the regionalization approaches are different.

Figure 3.3 shows that the regional mean and variability (mean ± standard deviation) for the selected attribute variables for each month between October and April, indicating that each region can be uniquely characterized based on their magnitude and temporal variation. For example, region 4, which includes coastal regions of Washington, Oregon and Northern California, is characterized by maritime climate

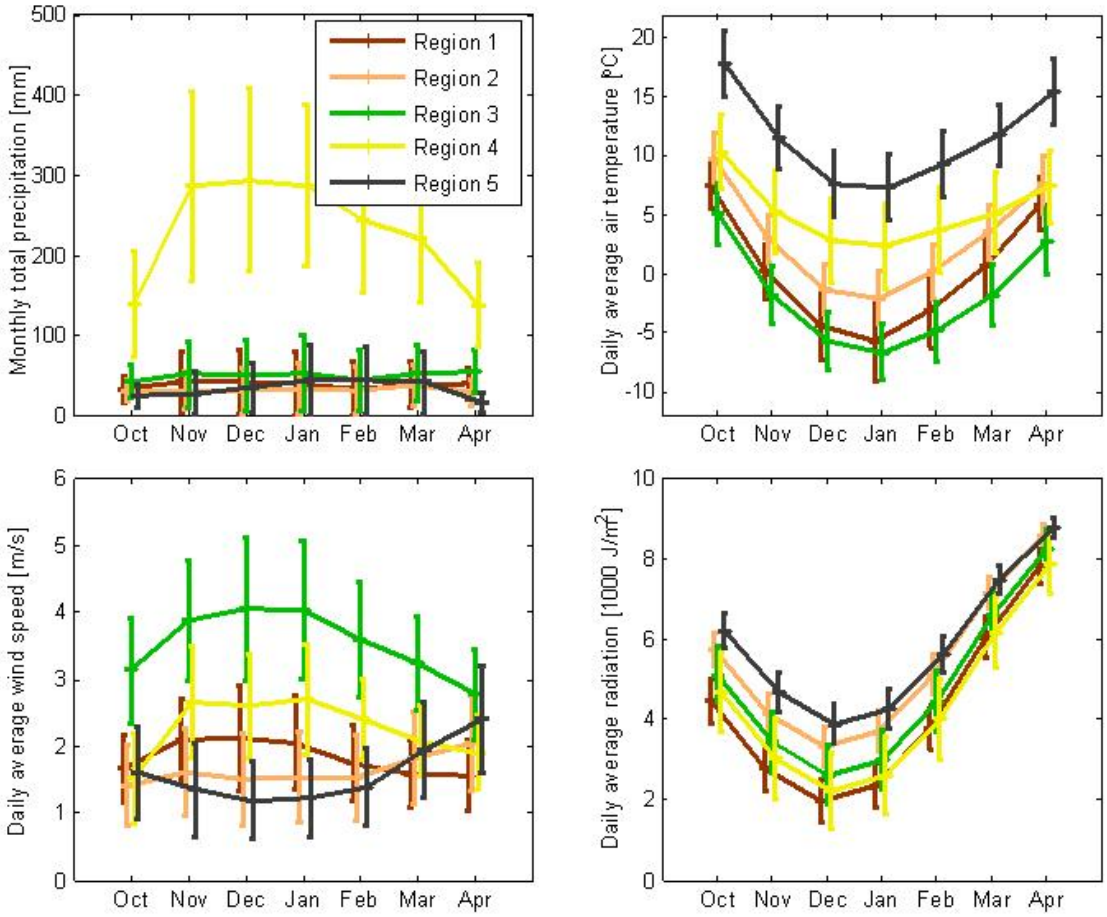

Figure 3.3. Monthly mean and variability (mean ±standard deviation) for total precipitation, daily average temperature, wind speed and radiation for each month from October through April for regions 1 to 4.

with exceptionally high precipitation amounts and high air temperature. Region 3, located in continental areas over Wyoming and eastern Colorado, is characterized by average wind speeds that are higher than in any other regions throughout the winter season. Because the wind speed data were available at a 32-km grid, the region 3 grids appear coarser than the grids inside other regions. Region 1 is similar to region 3 in terms of selected meteorological characteristics, except that average wind speeds are much lower in region 1 for all months. Similarly, regions 2 and 5 can be

distinguished based on air temperature; average daily temperatures are significantly higher in region 5 than in region 2 throughout the winter season.

3.4 Development and validation of regional equations for estimation of monthly climatological SWE grids

To estimate monthly climatological SWE distributions, a forward-selection stepwise regression was used for each region and each month between October and April. Forward-selection stepwise regression is a systematic method for adding predictors to a multilinear regression model based on their statistical significance in a regression [*Wilks*, 2005]. This method starts with an intercept-only model. In each consecutive step, all remaining predictors are screened for degree of their linear relationship with the predictand and one predictor that produces the highest coefficient of determination is added to a linear equation. This screening process is terminated when none of the remaining variables is significant at a certain level (95% was used in this study). The quality controlled daily SWE values at the SNOTEL sites were used to calculate monthly SWE changes (i.e., difference between SWE values on the first day and the last day of month) for each month from 1980 to 2004. They are then averaged over the 25-year period to obtain climatological monthly SWE changes, which were used as predictants for the regression analysis. The same geographic and meteorological variables considered for the regional delineation were tested as potential predictors of the climatological monthly SWE changes. For similar reasons discussed in Section 3.3 for cluster analysis, multicollinearity in explanatory variables was investigated and accounted for in variable selection. Climatological monthly SWE changes estimated via the calibrated regression equations were then accumulated at the end of each month between October and April to develop climatological monthly SWE grids. When the estimated SWE value for a grid cell became zero or below, it

was assumed that the snow pack completely melted during that month and a zero value was assigned to that grid cell.

To examine how the number of the regions affects performance of the regionally-calibrated equations, RMSE and R statistics were computed for climatological monthly SWE changes for varying number of regions. Average statistics across all regions, for 2-, 5- and 10-region cases, are shown in Table 3.2. As can be seen from the table, the increase in number of regions from 2 to 5, on average, significantly improves the accuracy of the estimates particularly in early to midwinter (October to March). However, the selected performance statistics are comparable for the 5- and 10-region cases for all the months but April. For comparison, the regional equations were also developed for the four regions delineated by *Sturm et al.* [1995]. As can be seen from the table, RMSE and R statistics for this regionalization approach are comparable to the 5-region case, except for February and April when the 5-region case performs slightly better.There was an additional reason in this study for keeping the number of the regions relatively small; as the number of the regions increased, the number of the measurement sites within each region decreased, leaving more and more regions with no SNOTEL sites. Even for the 5-region case, there are no SNOTEL sites in region 5 that encompass lower elevation areas in Southern California through Arizona/New Mexico (see Figure 3.1). As a result, the regional equations could not be calibrated for that region, but because of high temperatures and little precipitation as shown in Figure 3.3, significant snow accumulation is not expected in this region. Based on these results, the 5-region case grid classification was used to develop climatological monthly SWE grids over the western U.S.

For 5-region case, the overall performance of the developed equations can be seen from the performance statistics shown in Table 3.2. As a rule, 65 to 85% (R = 0.8-0.93) of observed monthly SWE change variability is explained through this model,

Table 3.2. Root mean squared error (RMSE; mm) and correlation coefficient (R) between measured and estimated climatological monthly SWE changes averaged aross the western United States for 2-, 5-, and 10-region cases from this study and for four regions as delineated by *Sturm et al.* [1995] for each month between October and April

		RMSE (mm)		
Month	**2-regions**	**5-regions**	**10-regions**	**Sturm**
Oct	9.19	7.90	8.00	8.08
Nov	27.89	17.76	17.79	18.13
Dec	30.72	21.75	21.41	21.70
Jan	33.37	22.32	21.33	22.21
Feb	28.85	20.06	19.52	21.60
Mar	36.24	31.77	31.23	31.12
Apr	63.49	65.03	57.85	68.98

		R		
Month	**2-regions**	**5-regions**	**10-regions**	**Sturm**
Oct	0.84	0.88	0.87	0.87
Nov	0.80	0.93	0.93	0.92
Dec	0.85	0.93	0.93	0.93
Jan	0.82	0.93	0.93	0.93
Feb	0.91	0.91	0.91	0.89
Mar	0.84	0.88	0.89	0.88
Apr	0.73	0.72	0.73	0.68

except in April, especially in regions 2 and 4 where R is less than 0.6. RMSE is also relatively small for the winter months in all the regions, but in April RMSE increases drastically for all the regions.

Table 3.3 also shows the coefficients of the regression equations for each geographic and meteorological variable in each month and region that were found to be statistically significant predictors of SWE change at the 95% significance level. Because the coefficients were determined for the standardized variables (see equation 1), they can be used to evaluate the relative significance of each variable in determining the SWE change variability; the larger the magnitude of the coefficient, the more significant the variable. As expected, precipitation is the most statistically significant predictor

Table 3.3. Root mean squared error (RMSE; mm) and correlation coefficient (R) between measured and estimated climatological monthly SWE changes averaged aross the western United States for 2-, 5-, and 10-region cases from this study and for four regions as delineated by *Sturm et al.* [1995] for each month between October and April

Region	Month	Latitude	Longitude	Elevation	Precipitation	temperature	Wind speed	Radiation	R	RMSE
	Oct	0.72	0.12	0.99	0.34	-	-	-	0.89	7.28
	Nov	0.30	-	0.60	0.84	-	-	-	0.91	14.89
	Dec	-	-	0.25	0.93	-	-	-	0.90	17.30
1	Jan	-	0.16	-0.09	0.94	-	-	-	0.93	16.04
	Feb	-	-	0.39	0.80	-	-	-	0.90	17.59
	Mar	0.60	-	0.86	0.52	-	-	-	0.89	29.65
	Apr	0.82	0.21	1.07	-	-	-	-	0.73	64.15
	Oct	-	-	-	0.39	-0.58	-	-	0.77	7.26
	Nov	0.50	-	0.54	0.71	-	-	-	0.93	13.82
	Dec	-	-	-	0.85	-0.27	-	-	0.89	20.06
2	Jan	-	-	-	0.81	-0.33	-	-	0.86	22.64
	Feb	0.61	-	0.69	0.67	-	-	-	0.90	20.02
	Mar	0.80	-	0.78	0.40	-	-	-	0.89	33.58
	Apr	-0.24	-	-	-	-	-	-	0.24	74.78
	Oct	-	-	-	0.57	-0.51	-	-	0.84	9.26
	Nov	-	-	0.18	0.90	-0.22	-	-	0.91	14.80
	Dec	-	-	-	0.92	-0.11	-0.08	-	0.92	15.34
3	Jan	-	-	-	0.94	-0.08	-	0.07	0.93	15.31
	Feb	-	-0.13	0.13	0.93	-	-	-	0.90	15.71
	Mar	0.66	-	0.69	0.70	-	-	-	0.83	23.34
	Apr	0.28	-	-0.22	0.28	-0.22	-	-	0.85	45.73
	Oct	0.74	-	0.98	0.19	-	-	-	0.87	9.45
	Nov	0.71	-	1.04	0.42	-	-	-	0.88	31.22
	Dec	0.48	0.29	0.92	0.51	-0.27	-	-	0.86	37.65
4	Jan	0.67	-	0.95	0.39	-	-	-	0.85	40.82
	Feb	0.51	-	1.03	0.36	-	-	-	0.87	31.68
	Mar	0.74	-	0.94	0.34	-	-	-	0.86	46.54
	Apr	0.30	-	-	-	-0.44	-	-	0.55	88.48
5	no SWE available									

for all regions during cold months. The inclusion of elevation becomes more important for the warmer regions or late winter month (March and April). Wind speed and solar radiation are not statistically significant predictors. Unexpectedly, air temperature does not explain SWE change even for the warmer months such as April. Possible explanations for the exclusion of air temperature in the regional equations are its relatively high correlations with latitude and elevation (see Table 3.1), both of which are identified as more statistically significant SWE predictors through the forward-selection stepwise regression approach.

The developed regional regression equations were further evaluated based on errors of climatological monthly SWE estimated using a jack-knife technique [*Papamichail and Metaxa*, 1996]. For each region and for each month, the regression equation was recalibrated for each site in the region without changing the type of regression equation or predictor sets included in the original equation, but with the data for that site excluded from the calibration dataset. Errors were computed by taking the difference between climatological SWE estimated from measurements and climatological SWE estimated through the jack-knife procedure at all the sites. Distributions of the errors in the estimated monthly SWE climatology for each region are shown in Figure 3.4. Since the error distributions were similar for the cold months (October through March), combined histograms for those months are shown in the figure for each region, and separate histograms are shown for April. As can be seen from the figure, in regions 1 to 3, errors are negligible at approximately 60% of sites and they are between ± 75 mm for more than 90% of sites. The magnitude of the errors in region 4 is typically larger than in the other regions throughout the season; they are negligible for approximately 35% of sites, and for approximately 70% of sites they are less than 75 mm. However, the error spread increases significantly for all regions in April, when the error magnitudes become too large ($> 75\%$) for at least 20-30 percent

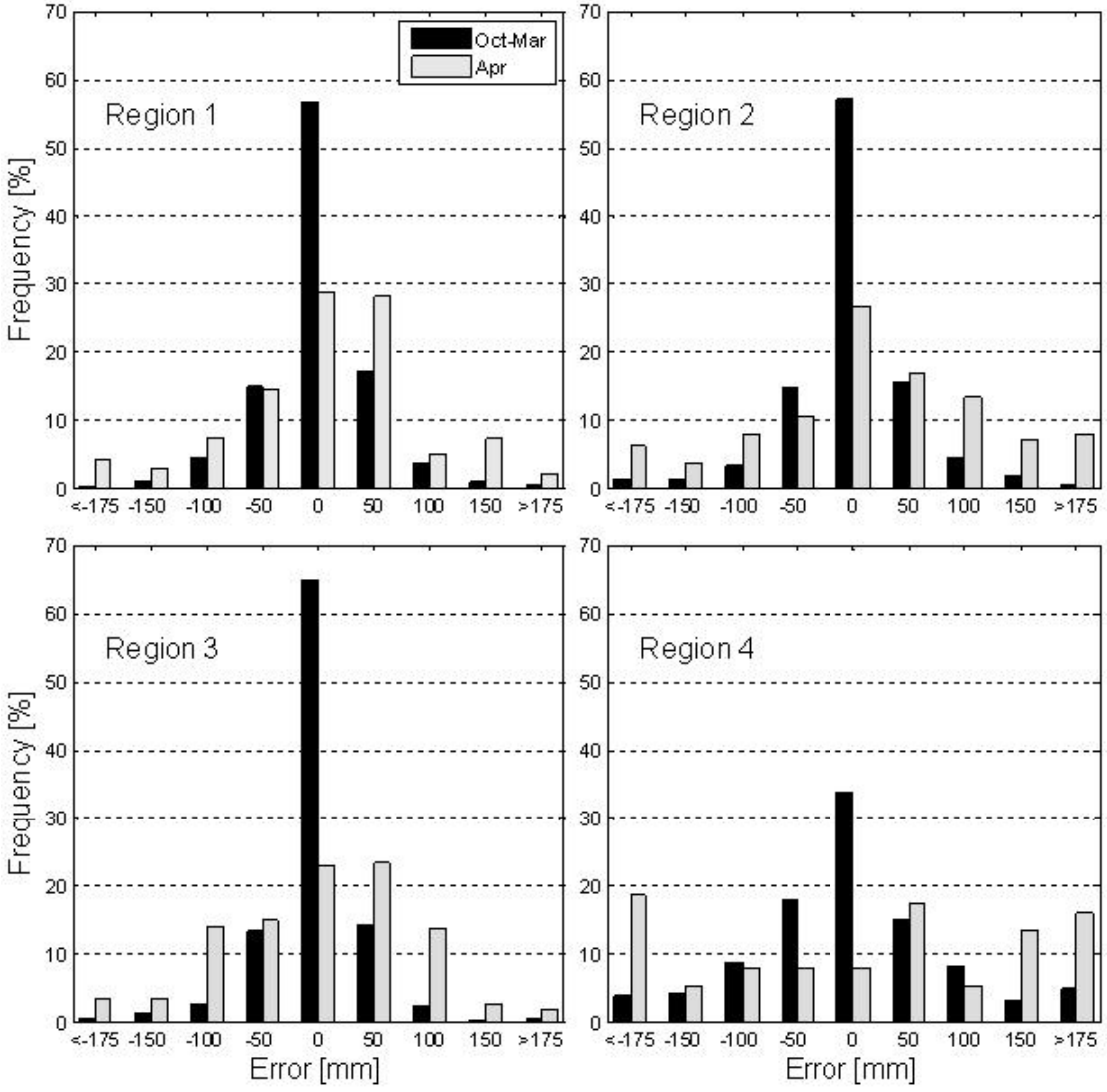

Figure 3.4. Error distributions for monthly climatological SWE estimated via jack-knifing for each region.

Table 3.4. Average regional climatological SWE (mm) together with performance statistics based on the jack-knife validation for each month and region

Month	Average regional SWE (mm) for region				RMSE (%) for region				Bias (%) for region			
	1	**2**	**3**	**4**	**1**	**2**	**3**	**4**	**1**	**2**	**3**	**4**
Oct	17.9	12.5	25.7	21.3	41	58	35	44	2	1	1	3
Nov	92.4	71.3	102.6	155.2	21	26	20	25	0	0	0	0
Dec	187.8	149.7	183.5	342.1	18	24	18	20	0	0	0	0
Jan	284.8	234.9	267.0	525.7	16	24	17	20	0	0	0	0
Feb	366.5	315.3	345.0	660.4	17	22	17	21	0	0	0	0
Mar	415.5	337.9	418.8	744.6	20	27	18	23	0	0	0	0
Apr	314.8	219.3	367.4	624.5	29	53	25	31	2	4	0	1

of the sites. To summarize the results, relative RMSE and bias of errors for each month and region are calculated and shown in Table 3.4 together with average regional climatological SWE estimated from SNOTEL measurements. As expected, there is very little bias across all the regions and for all the months. Relative RMSE is larger for October and April than for the other months when it is approximately 20%. Since there is very little SWE in October, that error is acceptable; however, that is not the case for April.

Finally, the spatial maps of SWE climatology for the mountainous regions of the western United States were generated; January and April maps are shown in Figure 3.5. The estimated patterns are predictable and qualitatively reasonable. A larger area of the western United States is covered with snow in January than in April, but the SWE magnitudes are greater in April when the significant amounts of SWE are concentrated in the higher elevation areas.

3.5 Summary and discussion

In this study, a regional regression-based approach for mapping SWE climatology for the mountainous regions of the western United States was investigated. To develop

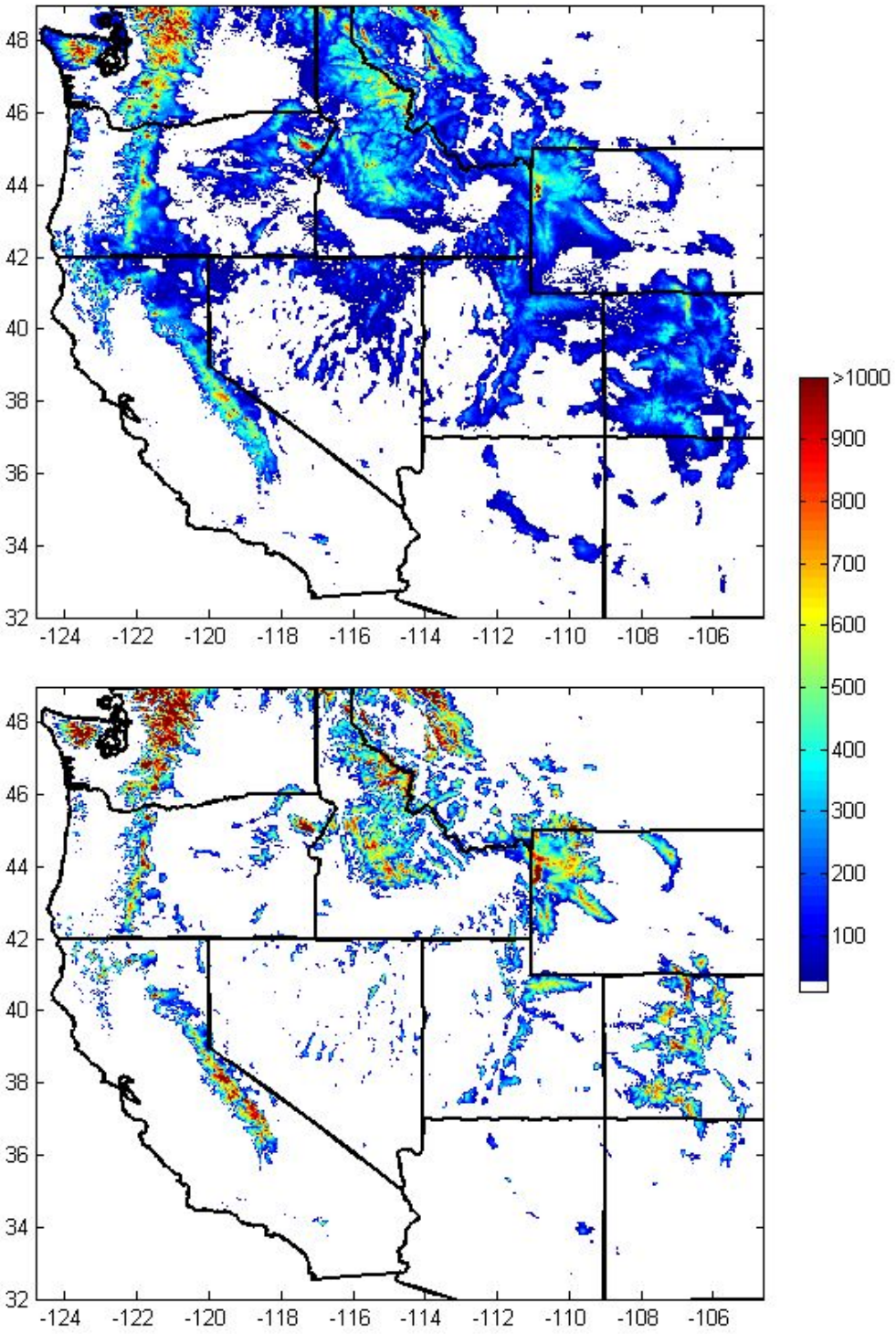

Figure 3.5. Spatial distribution of climatological SWE on January 31st (top) and April 30th (bottom). The maximum climatological SWE for the study area in January was 1650 mm, and 2690 mm in April.

climatological SWE grids, the entire western U.S. was first partitioned into five regions through cluster analysis with selected meteorological gridded data averaged between 1980 and 2004 used as SWE attribute variables. Forward-selection stepwise regression analysis, with at-site measurements of monthly SWE change averaged between 1980 and 2004, as a predictant and the corresponding selected geographic and meteorological variables averaged between 1980 and 2004 as predictors, was used to calibrate the regional equations for each month between October and April for each of the four regions where the SNOTEL stations were available. The developed regional equations were used to estimate climatological monthly SWE changes on a 4-km grid. They were further accumulated at the end of each month between October and April to develop climatological SWE grids.

The space-time resolution for this study (4 km and 1 month) was selected based on the resolution of readily available precipitation and temperature grids. Since the equations were calibrated for the specific regionalization and combination of space and time scales, the developed equations are not directly transferable to other spatio-temporal scales. In other words, for different regionalization schemes and different combinations of space-time scales, the regression equations have to be recalibrated. As such, the findings of this study should be considered solely for guidance. This study showed that even with relatively large regions and with a monthly time step, the estimation errors in the cold months when precipitation directly contributes to SWE increases are acceptable for the practical applications. However, for the given scale, the estimation errors become large when SWE starts decreasing (April for some areas in the western U.S). The monthly time step is definitely not adequate for the warmer months when the snow accumulation and ablation phases are contained in a single step. The analysis similar to this study would benefit if data were analyzed at a finer temporal scale, such as biweekly or even daily. Recently developed multiyear daily

meteorological grids on a continental scale [e.g., *Di Luzio et al.*, 2008; *Nelson et al.*, 2010] seem to be a promising source of high spatio-temporal resolution meteorological data that could be used in the future in a similar type of study.

Finally, it is worth mentioning some practical applications for which climatological SWE grids may be useful. One of their most important applications is in a bias correction of real-time SWE grids indirectly obtained from passive microwave data, airborne gamma measurements or various snow pack models. For microwave based estimations of SWE, for instance, those biases can be significant, especially in complex terrains, forested areas, and in proximity to water bodies [e.g., *Derksen et al.*, 2003; *Dong et al.*, 2005] and they have to be quantified and removed before real-time SWE data are used as input to hydrologic models. The bias correction can be achieved through statistical method such as the quantile-based matching method [e.g., *Reichle and Koster*, 2004; *Li et al.*, 2010], namely a statistical comparison of cumulative distribution functions of climatological SWEs obtained from in situ measurements and corresponding SWEs estimates.

Climatological SWE grids could also assist in statistical estimations of daily SWE amounts at ungauged locations. For example, the so called Mountain mapper technique [*Schaake et al.*, 2004] combines standard interpolation techniques (e.g., an inverse distance weighting) of at-site measurements of variable of interest (SWE, precipitation, etc.) with its gridded climatological estimates to obtain estimates at ungauged locations. This technique has been used for years in the National Weather Services River Forecast System for estimation of precipitation amounts at ungauged locations and it has proven to be superior to direct interpolation techniques, especially for applications over large basins in mountainous regions.

CHAPTER 4

EVALUATION OF PASSIVE MICROWAVE SWE RETRIEVAL ALGORITHMS OVER THE COLORADO RIVER BASIN

4.1 Introduction

The analyses in this chapter intended to characterize the estimation errors in various SWE retrieval algorithms by comparing daily SWE estimates from the algorithms with SNOTEL SWE measurements at the pixels that encompass the SNOTEL sites for each winter month. Several mountain ranges in the Colorado River basin were focused instead of the whole western United States.

The rest of chapter is organized as follows. The study area and the datasets used are described in Section 4.2. Section 4.3 starts with evaluation of the accuracy of SWE estimates from the original Chang's equation (Section 4.3.1) and then estimation errors were evaluated for successively calibrated SWE retrieval equations. The calibration included rending the grain coefficient of the Changs equation dynamic in time and space (Section 4.3.2) and using differences in TB from different combinations of channels (Section 4.3.3). Effectiveness of a statistical postprocessing of the SWE estimates from the all types of the algorithms in reducing their estimate errors was investigated in Section 4.4. Finally, findings and recommendations are discussed in Section 4.5.

4.2 Study area and datasets used in the study

4.2.1 Study area

The study focuses on seven major mountain ranges in or near the Colorado River Basin (Figure 4.1): the Wasatch Range and Uinta Mountains in Utah, Park Range, Front Range, and San Juan Mountains in Colorado, Wind River Range in Wyoming, and the Mogollon Rim in Arizona/New Mexico. The total basin area is 623,000 km^2 with an elevation range of 0-4260 m. For all of the mountain ranges in the study area, except the Mogollon Rim where snowfall constitutes 40% of annual precipitation, over 60% of the annual precipitation falls as snow [*Serreze et al.*, 1999].

4.2.2 Passive microwave data

The brightness temperature data used in this study come from the SSM/I instruments carried by the Defense Meteorological Satellite Program satellites. The SSM/I is a seven-channel, four-frequency, orthogonally polarized, passive microwave radiometric system that measures atmospheric, ocean and terrain microwave brightness temperatures at approximately 19, 22, 37, and 85 GHz frequencies [*Hollinger et al.*, 1990]. The SSM/I passes the Colorado River Basin area between 5:00-8:00 a.m. (morning path) and 5:00-8:00 p.m. (evening path) in local time. To reduce the possible influence of wet snow on the estimates, only TB data from the morning satellite paths were used for this study. Short periodic gaps in the daily dataset exist, as the 1,400km-wide SSM/I swaths do not always cover the study area. The data are available at Equal Area Scalable Earth Grid (EASE-Grid; approximately 25 x 25 km for the study area) developed by the National Snow and Ice Data Center [*Armstrong and Brodzik*, 1995]. TB data from the 17 winter seasons (October 1987 - April 1988 through October 2003 - April 2004) were used in this study.

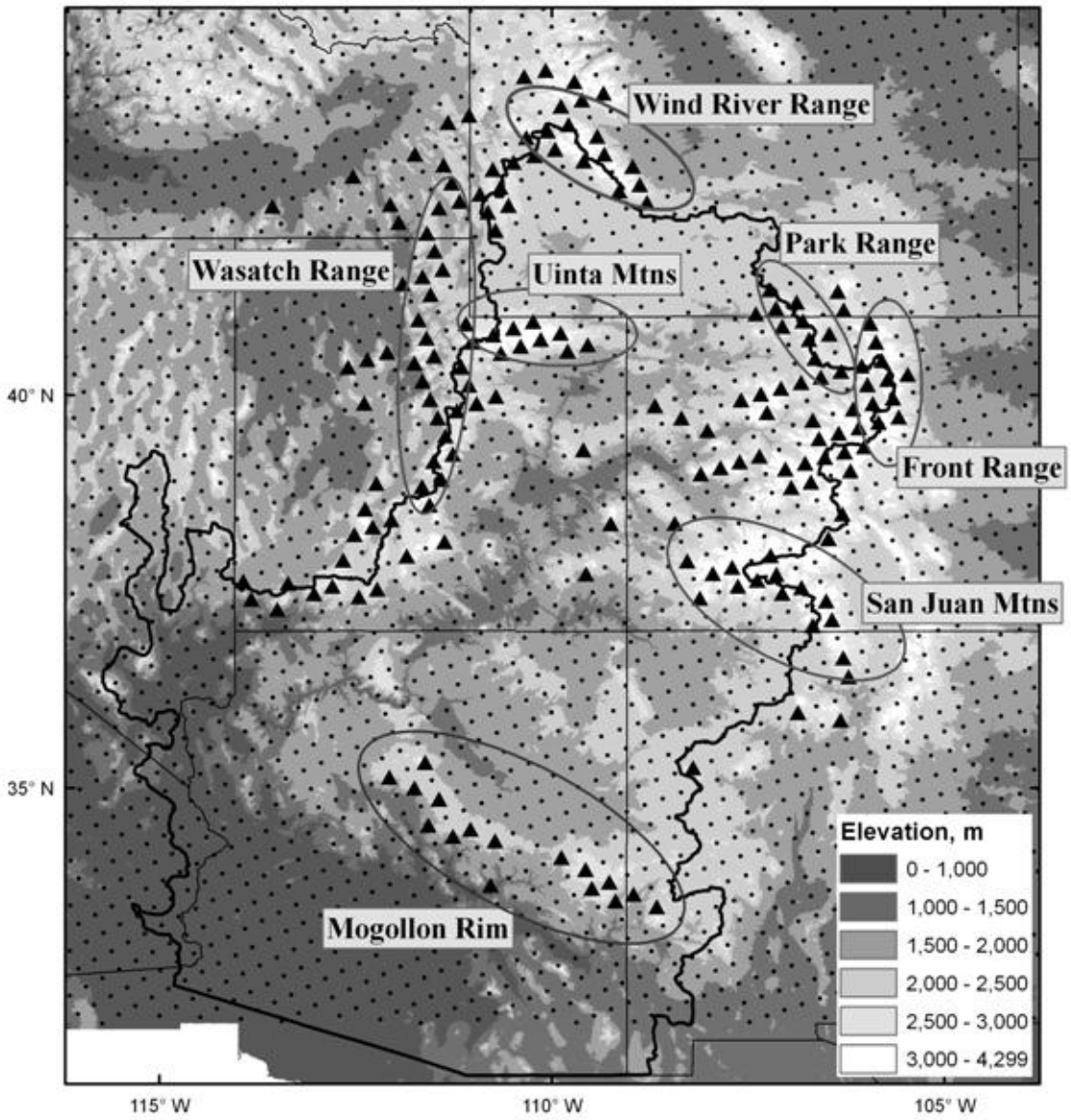

Figure 4.1. Colorado River basin with major mountain rages. Dots indicate centers of EASE-Grid cells. The cells with at least one SNOTEL site are shown as triangles.

4.2.3 SWE data

Daily SNOTEL SWE data from 1987 through 2004 were available at 262 sites in the study area, contained in 173 EASE-Grid cells (see Figure 4.1). As in Chapter 3, the SWE data were screened to perform quality control described in the Appendix.

4.3 Evaluation of PM SWE retrieval equations

Three SWE retrieval algorithms were successively evaluated at locations where in-situ measurements were available. The evaluation started with the Chang equation, which is, despite being one of the oldest algorithms, among the very few algorithms that have been used and evaluated in mountainous regions. An attempt was then made to improve the performance of this algorithm first through calibration of the equation's grain coefficient (hereafter calibrated Chang equation), and then by inclusion of various TBDs as SWE predictors (hereafter multi-TBD equation). Analysis was performed for each month between November and April separately to account for temporal changes in snowpack properties; a monthly time step was selected primarily for convenience and more efficient comparison of results. Two basic statistical measures, systematic bias and root mean square error (RMSE), were selected to quantify the errors in daily SWE estimates from the three algorithms and to make comparisons between results.

4.3.1 Chang's equation

In Figure 4.2, systematic bias (left panels) and RMSE (right panels) are shown for the SWE estimates from the Chang's equation for each location for November, February and April, representing early, middle and late periods of the winter season, respectively. As seen in the left panels in the figure, the SWE amounts are consistently underestimated across the study area throughout the season. The magnitudes of both error measures are generally higher for Wasatch Range in Utah and Park Range in

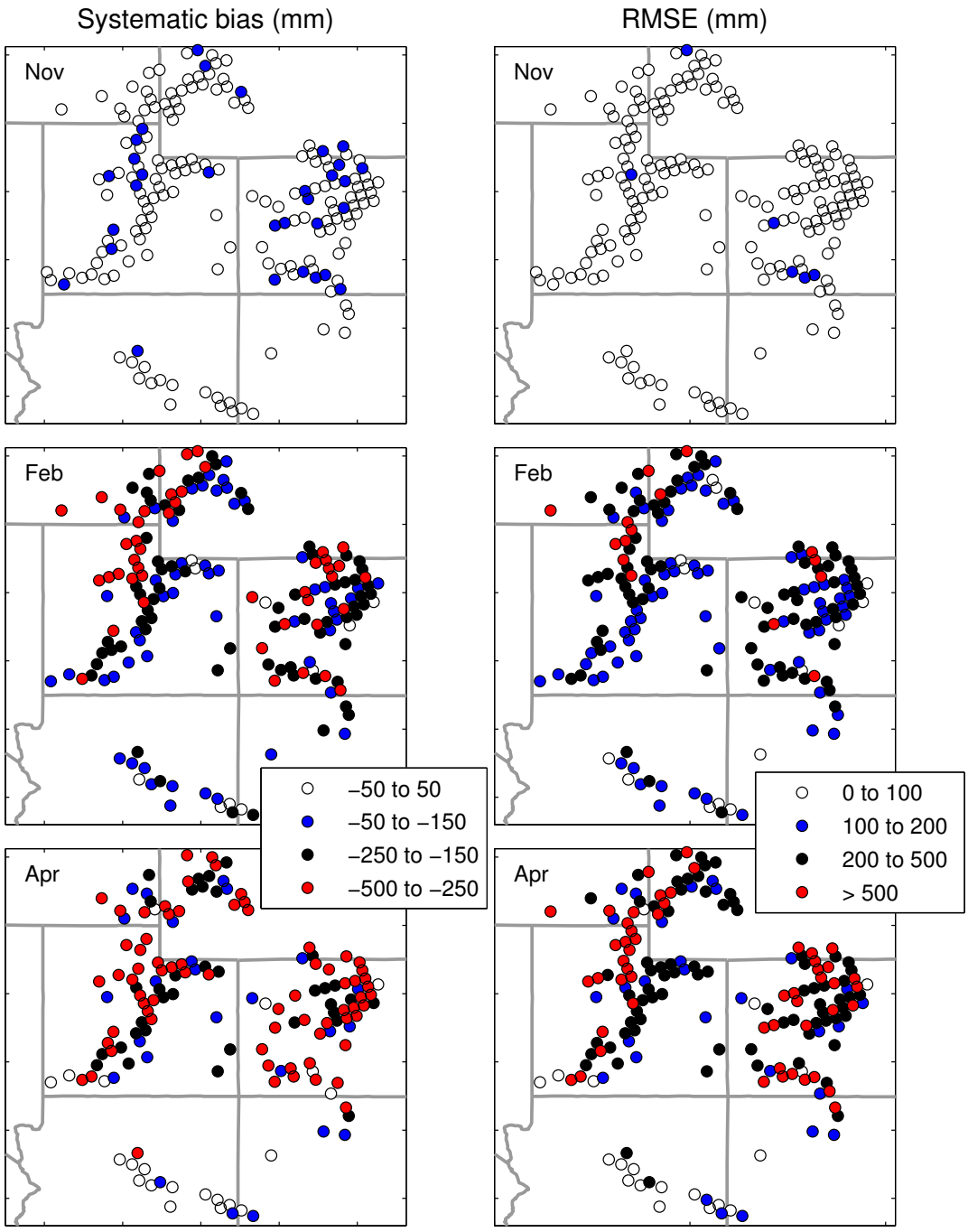

Figure 4.2. Systematic biases (left panels) and RMSEs (right panels) for SWE estimated from the Chang's equation at each location for November, February and April

norther Colorado than for the other mountain ranges.

Both error metrics increase across the study area during the winter season without a corresponding change in spatial patterns. The negative bias is, on average, about 300 mm for the whole area, and surpasses 500 mm in April at several locations. The average RMSE for the area is over 200 mm from February until April with a sizable number of locations featuring RMSE values above 500 mm. These calculated biases are comparable to the biases reported in a similar analysis done by *Dong et al.* [2005] for the mountainous regions in Canada. In their study, seasonal average errors in SWE estimates from the Chang's equation, relative to in-situ SWE measurements, exceeded 200 mm for numerous areas.

4.3.2 Calibrated Chang's equation

An attempt was made to improve the Chang algorithm performance through calibration of the grain size coefficient, which has a fixed value of 4.8 in the original equation. As previously mentioned, this coefficient value was derived under the assumption of dry snowpack condition with a constant grain size of 0.3 mm and a constant snow density of 300 kg/m^3 over open areas. The postulation in this analysis was that calibrated coefficient could potentially account for the combined effects on microwave emissions of the physiographic characteristics and actual physical properties of the underlying snowpack. Over dense forest areas, for example, the coefficient value is expected to increase to overcome the mask effect of the forest on microwave emissions, while the coefficient value is expected to decrease for the snowpack dominated by larger crystals (depth hoar) to account for volume scattering that is causing SWE overestimation.

Since the Chang's equation is, in essence, a linear equation between the SWE as a dependent and the TB difference as an independent variable, with a zero constant term and the grain size coefficient representing the slope of the equation, zero-

intercept regression analysis can be used to find the optimal value of the coefficient for each location and month.

Coefficients were calibrated via a leave-one-year-out cross validation method using the 17 years of data. There was little difference among individual coefficient values; they were typically between ± 10% of the corresponding averages. Figure 4.3 shows 17-year average calibrated grain size coefficients at each location for each month between November and April. As can be seen from the figure, optimal coefficients are normally much higher than 4.8 mm/K used in the Chang's equation, except in November. Generally, coefficient values increase throughout the season, which corresponds to findings by *Foster et al.* [2005].

Because the zero-intercept linear regression model was used, as expected, systematic biases were not completely removed, but were greatly reduced at the majority of sites for all months. The scatter plots of RMSEs for SWE estimated from the original and calibrated Chang equation, shown in Figure 4.4 (black circles), indicate that RMSE values also greatly decreased at the majority of locations for all months. For the whole study area, the average, RMSE of the values from the calibrated equation is about 50% less than that produced by the Chang equation.

During the analysis, however, it became apparent that while zero-intercept regression model is guaranteed to produce the expected positive relationship between the SWE and TBD, the true relationship between the two is sometimes the opposite. As can be seen from Figure 4.5, Pearson correlation coefficients between the two variables are negative at numerous locations. In February, for instance, the coefficient is negative at approximately half of all sites clustered in the Colorado, Wyoming, and Uinta mountains. Figure 4.6 shows scatter plots of SWE and (TB_{18H}-TB_{37H}) throughout the winter at a location (38.49 N, 106.30 W) in the Front Range in Colorado. Both nonzero intercept and zero-intercept regression lines are shown in

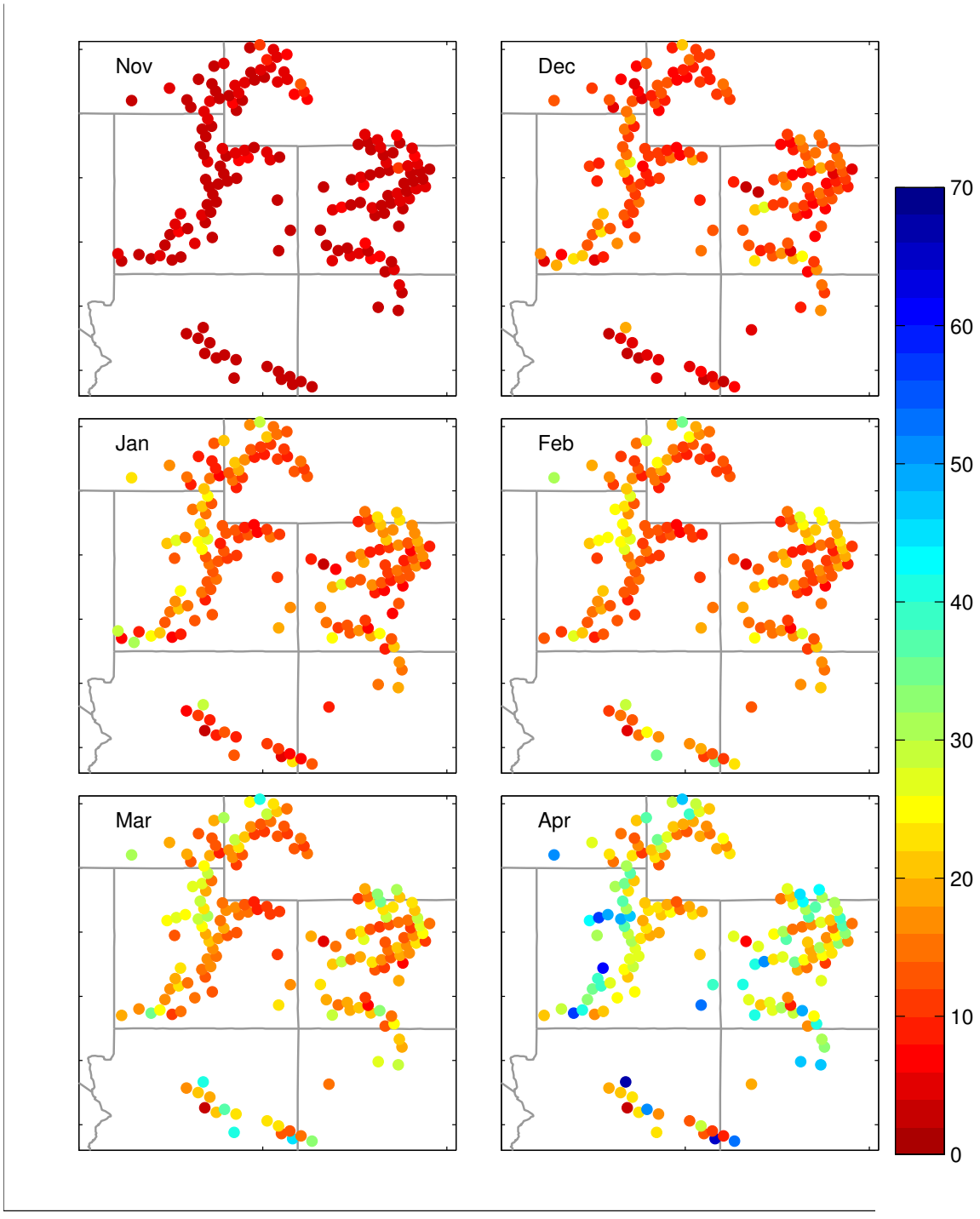

Figure 4.3. Average values for the calibrated grain size coefficients at each site per month

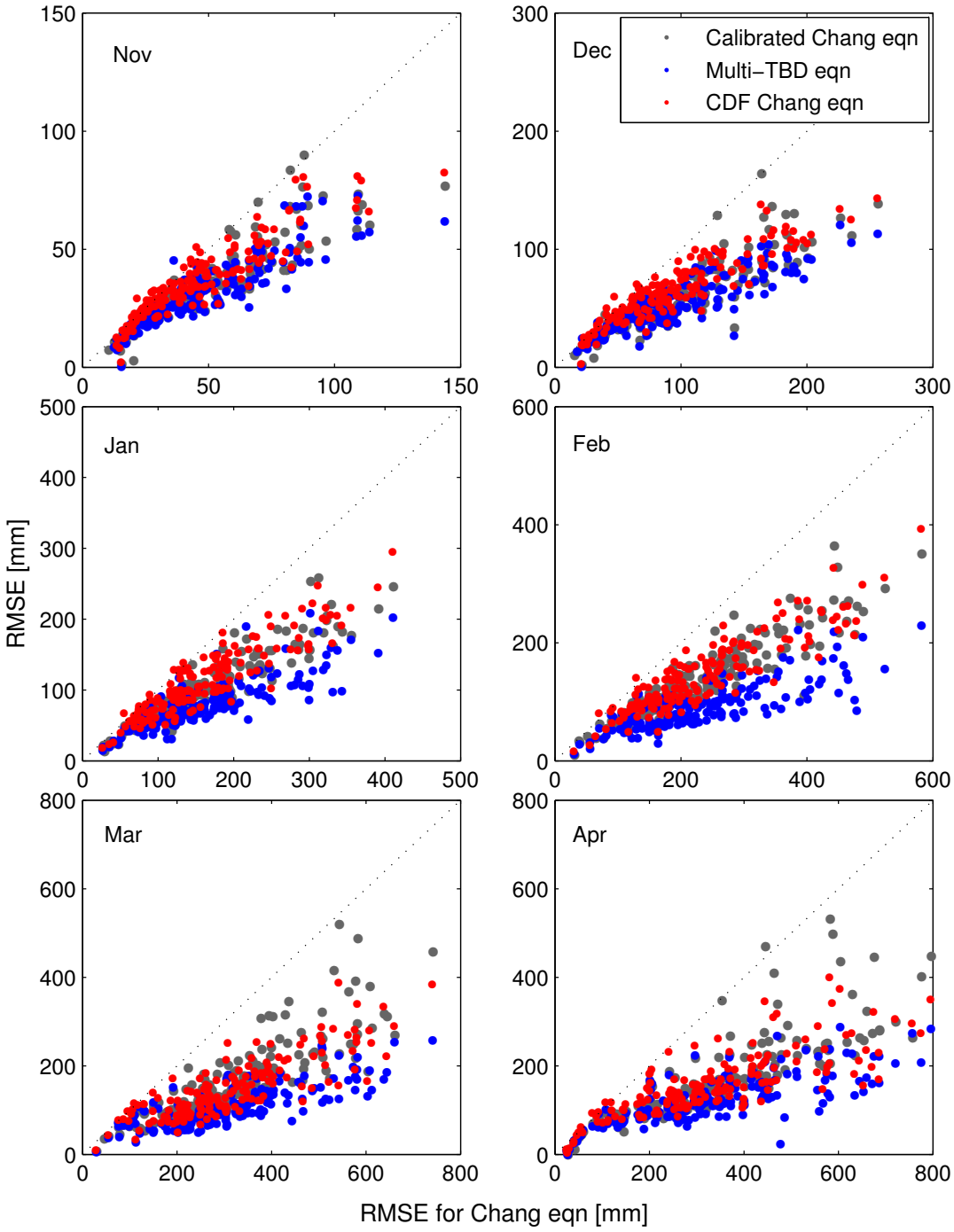

Figure 4.4. Scatter plots of RMSE in SWE estimates from the Chang's equation versus those from the calibrated Chang's equation (black dots), multi-TBD equations (red) and statistically postprocessed Chang's equation (blue).

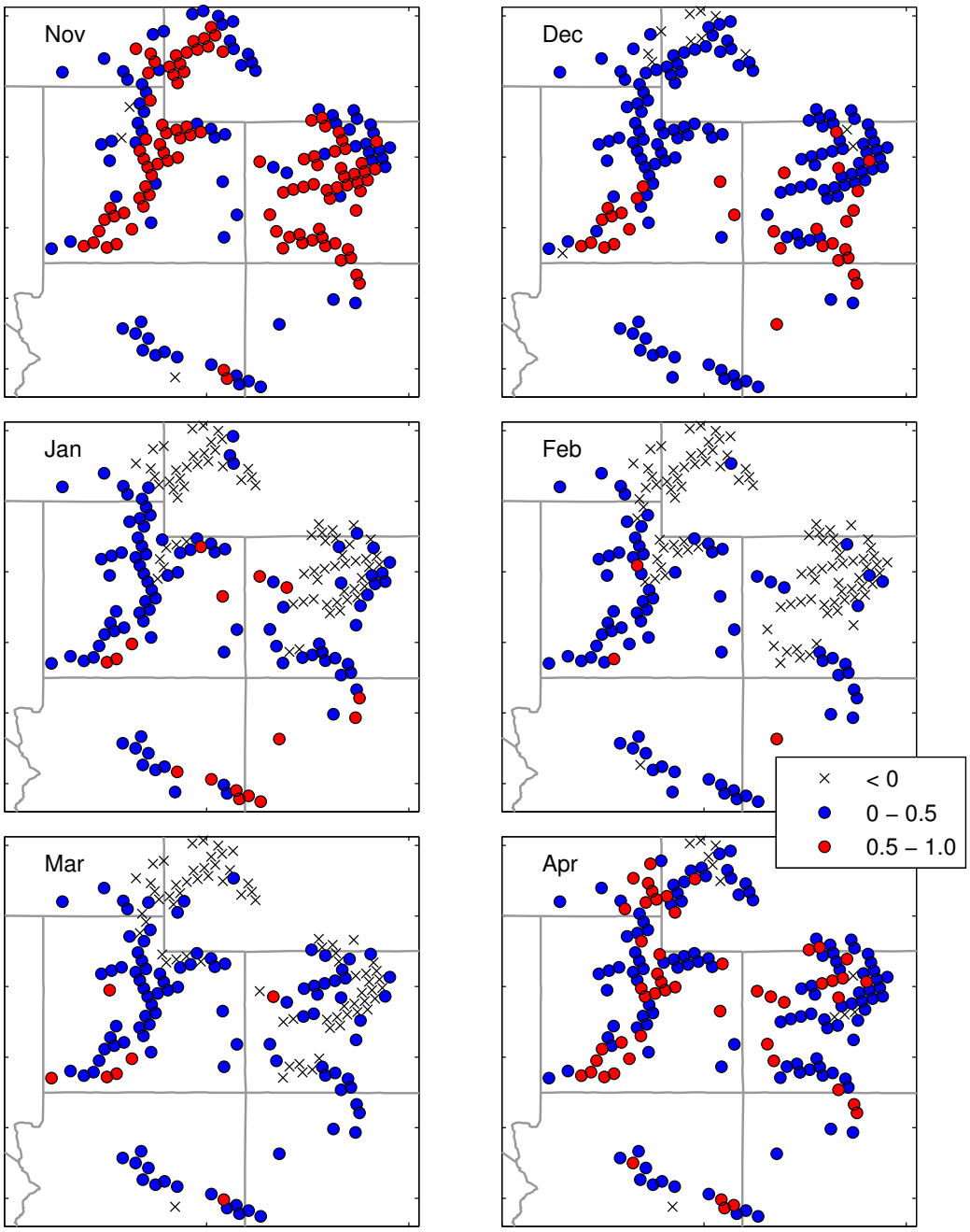

Figure 4.5. Pearson correlation coefficients between daily SNOTEL SWE measurements and (TB_{18H}-TB_{37H}) for November through April.

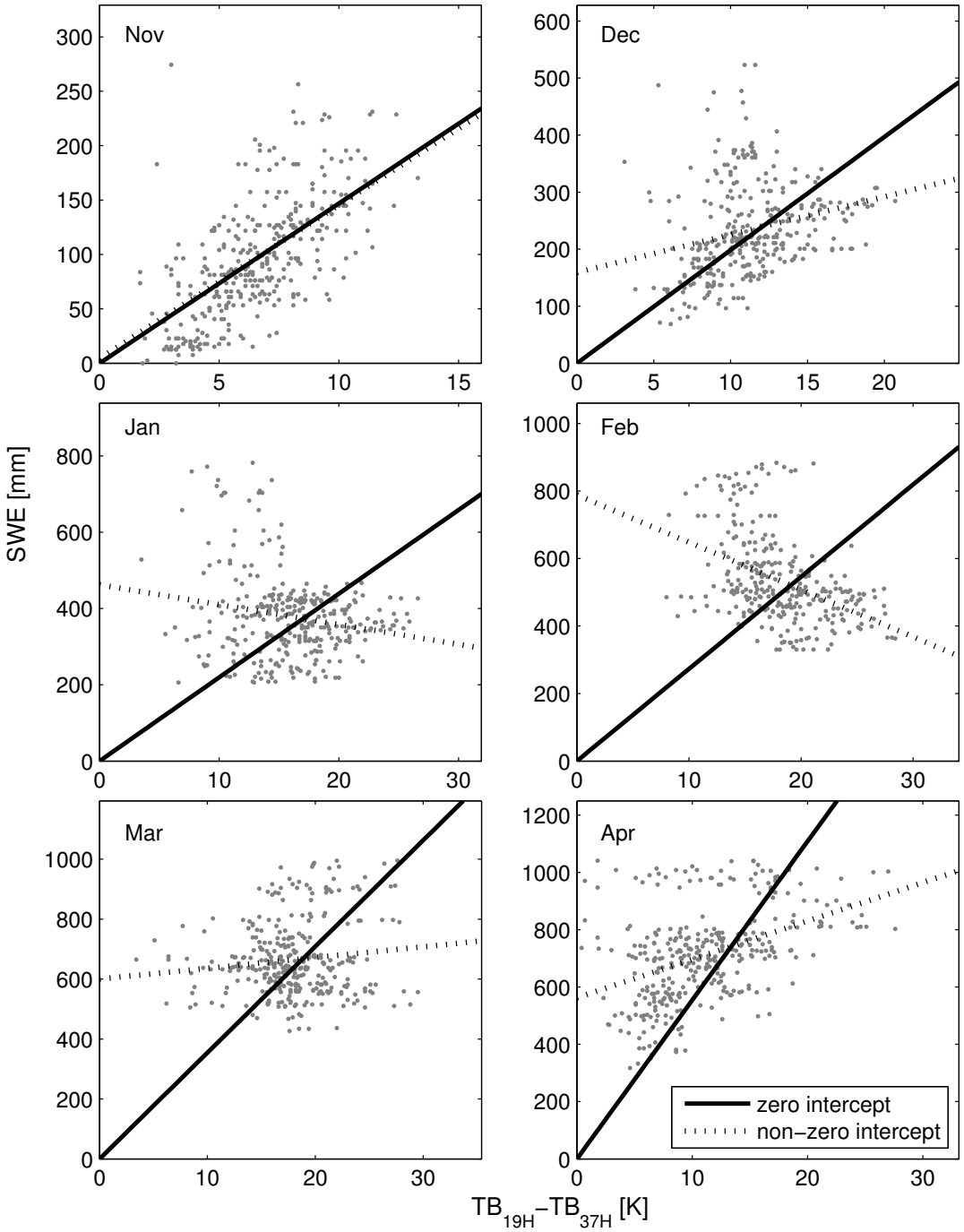

Figure 4.6. Scatter plots of SWE versus (TB_{18H}-TB_{37H}) together with linear regression lines with and without constraints on the intercept for a selected location (40.47 N, 106.65 W) for each month between November and April.

the figures. This reversed relationship likely occurs due to saturation of microwave emission for larger frequencies (in this case TB_{37H}) in deep snow or/and presence of large crystals in the snowpack.

4.3.3 Multi-TBD equation

Given the negative correlation between the SWE and (TB_{18H}-TB_{37H}) especially during cold months, different combinations of frequency channels were examined for potential improvement of the SWE estimates. Stepwise multivariate regression analysis with various TBD combinations as predictors was performed for each month and for each gauged location. In addition to the difference in TB measurements from the horizontally polarized channels, vertically and cross-polarized TBDs (one TB is horizontally polarized and another is vertically polarized) were also included in the analysis based on the findings of *Koenig and Forster* [2004] that polarization differences of both 85 GHz and 37 GHz were statistically significant predictors for depth-hoar dominated snowpack in the Alaska's North Slope. The 90% level was used as the demarcation for statistical significance. Table 4.1 shows the frequency of each TBD combination that ended up being statistically significant for each month. For example, cross-polarized TBD at 19 GHz was the most frequent statistically significant term throughout the season; it was statistically significant SWE predictor for 71% of locations in January. By comparison, in January, the TBD combination used in the Chang's equation was statistically significant only in 28% of cases. TBD combinations that included 85 GHz were significant predictors less frequently possibly due to emission saturation caused by deeper snowpack in this area. It should be noted, however, that at a given location, the set of statistically significant TBD terms developed via the one-year-out cross validation method greatly varied from year to year (not shown). As in the calibrated Chang's equation analysis, systematic bias and RMSE values were calculated using leave-one-year-out cross validation. This

Table 4.1. TBD combinations investigated as potential SWE predictors in stepwise regression analysis and frequency of each TBD combination (in percent) that ended up being a significant predictor at 90% significance level per month.

TBD	Nov	Dec	Jan	Feb	Mar	Apr
$TB_{19H} - TB_{19V}$	48	52	71	66	66	58
$TB_{19H} - TB_{37H}$	48	23	28	34	23	32
$TB_{19H} - TB_{37V}$	21	18	19	36	25	14
$TB_{19H} - TB_{85H}$	18	17	16	9	15	22
$TB_{19H} - TB_{85V}$	15	24	19	14	12	15
$TB_{19V} - TB_{37H}$	17	22	12	15	10	24
$TB_{19V} - TB_{37V}$	23	24	10	11	8	11
$TB_{19V} - TB_{85H}$	8	7	7	2	16	10
$TB_{19H} - TB_{85V}$	15	7	8	3	8	9
$TB_{37H} - TB_{37V}$	9	9	37	20	15	26
$TB_{37H} - TB_{85H}$	5	17	10	6	15	5
$TB_{37H} - TB_{85V}$	6	23	18	6	8	17
$TB_{37V} - TB_{85H}$	9	7	6	7	8	17
$TB_{37V} - TB_{85V}$	10	9	10	2	11	7
$TB_{85H} - TB_{85V}$	25	26	11	32	20	14

analysis, depicted in the scatter plots of Figure 4.4 (blue dots), showed that the use of optimized TBD combinations led to greater reductions in RMSE than did the calibration of the Chang's equation, particularly for February and March.

4.4 Evaluation of statistical postprocessing of SWE estimates from PM SWE retrieval algorithms

The effectiveness of statistically postprocessing the SWE estimates to reduce bias and RMSE through application of the cumulative distribution function (CDF) matching method (also known as a quantile matching method) was investigated. The CDF matching method has been widely used in various applications; for example, it has been used for bias correction in satellite estimates of soil moisture [*Reichle and Koster*, 2004] and precipitation [*Anagnostou et al.*, 1999], and for removal of biases in outputs from climate models [*Li et al.*, 2010] and from hydrologic models [*Wood et al.*, 2002].

The principle of the CDF matching is to first establish a statistical relationship between the estimates and observations based on their historical CDFs and then to adjust real-time estimates (or forecasts) by replacing them with observations that have the same nonexceedance probability. This procedure can be expressed mathematically as follows:

$$X_{adj} = F_{obs}^{-1}(F(X)) \tag{4.1}$$

where X is an estimate of a variable under consideration (in this case SWE estimated from the TB data), F_obs and F are nonexceedance probabilities of estimate X obtained from historical CDFs of observations and estimates, respectively, and X_{adj} is the adjusted estimate.

Since the CDF matching method does not depend on the algorithm used to derive the estimates, it was applied to SWE estimates obtained from all the SWE retrieval algorithms analyzed in Section 4.3. For each location and for each day between November 1st and April 30th, CDFs were constructed from SNOTEL SWE measurements and from SWE values estimated from microwave data by means of the Chang's equation, calibrated Chang's equation and multiple TBD equation using daily values over a 7-day period centered on a day of interest. To be consistent with the analyses in the previous section, RMSE and systematic bias were calculated using leave-one-year-out cross validation method. The CDFs for the observations and estimates were generated from the dataset with 1 year's data excluded and then used to adjust daily SWE estimates from the excluded year. The process was repeated 17 times, and every time a different year of data was excluded. Finally, adjusted estimates were compared with the SNOTEL SWE measurements from the excluded year to calculate bias and RMSE statistics. The CDF matching method proved to be very efficient in removing systematic bias and reducing the RMSE between 30 and 50%, when coupled with the Chang's equation (red dots in Figure 4.4). Statistical

postprocessing of results from the calibrated Chang's equation and the equation with multiple TBD was not beneficial. The estimates from those two approaches were relatively unbiased to start with, and statistical postprocessing did very little to reduce the RMSE. In fact, RMSE even slightly increased in a few cases.

4.5 Summary and discussion

To summarize the analyses, average monthly bias and RMSE statistics were calculated for the whole study area (Table 4.2). The Chang equation consistently underestimated SWE amounts. The average bias for the study area varied from -26 mm in November to almost -300 mm in March and April, exceeding -500 mm at some locations. The RMSE was also high; the areal average was well above 200 mm between February and April, exceeding 500 mm at numerous locations, and even reaching 800 mm at several sites. Through statistical postprocessing, biases were removed and RMSE was reduced by approximately 50% across the whole winter season. While the CDF matching technique is quite successful in reducing the estimation errors at locations with in-situ SWE measurements, it becomes less attractive for applications that require SWE estimates over large areas since a regionalization would be necessary for it to be usable at ungauged locations. One of the recommended approaches is an index-flood regional frequency analysis approach. The term index-flood comes from the method's first applications in flood frequency analyses [*Dalrymple*, 1960], but the method is applicable to any types of cumulative distribution analyses. The underlying assumption of the index-flood approach is that all locations in a homogeneous region have different climatological means but common normalized higher order statistics; therefore the CDF normalized by the climatological means is identical in the homogeneous region. The regional normalized CDF derived from gage data can be applied to ungaged locations as observed CDF (F_{obs} in Equation 4.1). *Mizukami et al.* [2011] developed monthly gridded SWE climatology map over the western United States

Table 4.2. Comparisons of basin-wide bias and RMSE for each SWE retrieval algorithm without and with statistical postprocessing (columns (1) and (2), respectively) for each month.

	Systematic bias (mm)					
Month	**Chang's eqn**		**Calibrated Chang' eqn**		**Multi-TBD eqn**	
	(1)	(2)	(1)	(2)	(1)	(2)
Nov	-26	0	-3	0	0	-1
Dec	-72	0	-8	0	0	-5
Jan	-129	3	-17	0	1	-8
Feb	-199	-1	-29	0	-1	-9
Mar	-280	-2	-43	-2	0	-6
Apr	-283	-4	-43	-2	0	-7

	RMSE (mm)					
Month	**Chang's eqn**		**Calibrated Chang' eqn**		**Multi-TBD eqn**	
	(1)	(2)	(1)	(2)	(1)	(2)
Nov	44	37	34	37	31	32
Dec	90	67	59	66	53	53
Jan	154	114	101	114	81	78
Feb	225	148	140	146	93	97
Mar	302	151	164	151	109	115
Apr	316	159	164	159	124	130

based on regional regression analysis, which can serve climatological SWE means. To delineate homogeneous regions in terms of similar snow pack climate and physiographic characteristics that affect passive microwave emissions, regionalization approaches similar to approaches developed by *Farmer et al.* [2010] or *Mizukami et al.* [2011] could be used. Those two approaches are particularly attractive because they both used gridded data as input variables for cluster analysis; therefore the delineated regions are spatially continuous.

The error statistics significantly improved when the grain coefficients in the Chang's equation were calibrated at each measurement location; biases were reduced by approximately 85% and RMSEs were reduced by 40-50%. Since the calibration was

done for each month separately, temporal variations in the SWE - TBD relationship were also indirectly accounted for. The calibrated Chang's equation approach has several important advantages. First, it is a physically based algorithm. It is a particularly attractive approach for applications that require SWE estimates over large areas; a single coefficient in the algorithm that indirectly accounts for various factors affecting the relationship between microwave emission and SWE was found to be spatially coherent (Figure 4.3). Therefore, estimation of SWE grids covering extended areas could be as simple as interpolation of the grain size coefficient. A major concern in using this type of equation is that although the zero-intercept model produces the expected results, a forced relationship was not always borne out by the measurements. In fact, the observed SWE-TBD relationship was the opposite to expected for midwinter months at many locations in this study area. Through statistical postprocessing, it was possible to remove the remaining small biases, but the RMSE could not be further reduced. Because of that, in addition to the regionalization issues discussed above, the statistical postprocessing of SWE estimates using the CDF matching technique is not recommended.

The SWE retrieval algorithm that uses multiple TBDs produced unbiased SWE estimates. RMSEs were 50-60% less than those from the original equation, and were consistently smaller than the RMSEs associated with the calibrated Chang's equation. For that reason alone, this is the recommended SWE retrieval algorithm for single-site or small-scale applications, especially if SWE records are long enough to support reliable calibration. The algorithm is less attractive for applications that require spatially continuous SWE estimates over large areas because the extrapolation of results to ungauged location is not as straightforward as with the calibrated Chang's equation. One approach could be to develop regional equations using data from all stations inside of a homogeneous region. However, the regionalization approach

would indeed increase errors at gauged locations. There would be no regional biases, but estimates at each location would no longer be unbiased. At-site RMSEs would also likely increase. To gain insight into how much the model performance might deteriorate if the equations were regionally calibrated, the multi-TBD equations were developed treating the whole study area as one region. Table 4.3 compares the average RMSEs from equations calibrated separately at every gauged location to corresponding RMSEs from equations calibrated using all of the data for each month. As can be seen from the table, RMSE values increased by at least 50% and almost doubled in April. However, it is likely that if regional equations were developed for truly homogeneous regions, RMSEs would be smaller.

Finally, the analyses throughout this paper were based on comparisons of two different spatial scale SWE values (25 km x 25 km grid cell versus point). Obviously the SWE measured at a SNOTEL site is unlikely to represent areal mean SWE over the grid box in particularly for mountainous regions. Therefore, the calibration of the algorithm results in reproducing point SWE values at a particular location within the grid cells. Representativeness of point SWE measurements to the areal average values have been discussed in the past. *Chang et al.* [2005] concluded that more than 10 point measurements are required for reasonable representativeness of 1-degree box (error less than 50mm) over the northern great plain in the United States where topography, hence snowpack properties, are less heterogeneous than the Rocky Mountain areas. For the mountainous areas, *Molotch and Bales* [2005] examined the representativeness of six SNOTEL sites in Rio Grande located within the Colorado River basin to the surrounding grid boxes (1, 4, and 16 km scale). The bias of SWE from SNOTE compared to areal mean SWE can be positive or negative depending on the sites; in some case, it can be 200% greater than mean areal SWE. With the issues associated with representativeness of ground observed data, the calibrated Chang's equation

Table 4.3. Average RMSE (mm) from the Multiple-TBD algorithm for calibration done at each site and RMSE (mm) for regional calibration.

Month	RMSE (mm)	
	At-site calibration	Regional calibration
Nov	31	42
Dec	53	74
Jan	81	116
Feb	93	148
Mar	109	179
Apr	124	215

and multi-TBD equation will reproduce the SWE characteristics from SNOTEL rather than estimating areal average SWE. However, the in-situ SWE observation is expected to better represent the satellite grid cell with higher spatial resolution of the passive microwave radiometer. The latest microwave radiometer- the Advanced Microwave Scanning Radiometer Earth Observing System (AMSR-E), provide 20 km for 18.7GHz and 12km for 36.5GHz since 2002. The calibrations of the SWE retrieval algorithms presented in this study would be possible with longer AMSR-E dataset in the future.

CHAPTER 5

CONCLUSIONS

5.1 Summary

Quantitative information of spatial snow distribution is central to the understanding of terrestrial processes. Despite the significant amount of seasonal snowpack in mountainous areas, its large scale mapping is significantly more arduous than mapping of less complex landscapes, primarily due to higher spatial variability of snowpack in mountainous regions. This dissertation examined two potential approaches to deriving spatial and temporal distributions of snow volumetric variables over the mountainous regions of the western United States. SWE, which represents snow mass (and is therefore pertinent to hydrology) was a focused quantity for the analyses. The examined mapping methods are 1) spatial interpolation of ground-measured SWE; and 2) SWE estimation via passive microwave satellite. Summaries of all analyses are given here.

Climatological characteristics of seasonal snowpack were first examined for each SNOTEL site that provided both the SD and SWE snowpack volumetric variables between the 1999/2000 and the 2005/2006 winter seasons. The most significant finding is that in contrast to SWE and SD, snowpack density estimated from both SWE and SD exhibits less year-to-year variability compared to the change observed in SD and SWE throughout the winter season. With small interannual variability, reliable estimates of climatological values of snowpack density could be deduced at any location, using only several years of SWE and SD measurements. Real-time and retrospective estimates of SWE could be deduced by merging climatological snowpack

density data with denser networks of SD measurements, such as those obtained from National Weather Service (NWS) Cooperative Observer stations, as well as NWS First Order Stations. The complexity of spatial and seasonal variability of snow pack density was characterized using cluster analysis. Among several topographic and geographic variables, elevation and longitude appear to be explanatory variables which separate different snow density regions.

In Chapter 3, the procedure for the spatial interpolation of in-situ SWE measurements for gridded SWE mapping over the western United States was presented and the errors of interpolated SWE values were evaluated. The developed method was a simple but viable regional regression-based approach with readily available geographic and meteorological parameters used as predictors. This method was then used to map SWE climatology in the mountainous areas of the entire western United States. As a first step, the mountainous regions of the western United States were regionally delineated through k-mean clustering, using various climate parameters that influence seasonal snowpack accumulation and ablation processes as attribute variables. Various geographic and climate parameters were then investigated through stepwise regression in order to assess their potential as predictors of monthly changes in climatological SWE for each delineated region. Spatial and temporal resolution of the analysis was based on the resolution of available meteorological data - 4 km and 1 month, respectively. For a monthly time step, the reliability of the SWE estimates did not significantly increase when the number of regions evaluated was more than five. The regional equations that were developed using monthly resolution and a 5-region sample/case, provided reliable estimates for the majority of regions from October to March. For April however, based on cross validation analysis, the equations did not provide reliable estimates, especially in the North Pacific and Southwest regions. This climatological information is potentially useful for several applications, including

estimation of real-time SWE grids via the mountain-mapper technique, as well as calibration and/or evaluation of SWE estimates obtained from remote sensing or through various snow models.

In Chapter 4, the performance of three passive microwave SWE retrieval algorithms was examined over the mountainous Colorado River Basin by comparing daily SWE estimates from the selected algorithms with in-situ SWE measurements. Additionally, statistical postprocessing, namely CDF matching, was tested as a means of improving the SWE estimates from each retrieval algorithm. The standard Chang equation has been used for global scale SWE or SD mapping, but use of this algorithm on a regional scale, particularly a mountainous region, would be highly problematic, based on results which indicate a large negative bias (up to -300 mm) and RMSE (up to 500 mm) for numerous locations. Calibrating the grain size coefficient of the Chang equation with in-situ SWE data incorporates unique response of microwave emission to physiographic and snowpack characteristics for each location. As expected, the calibrated Chang equation reduced estimation bias greatly, and to a lesser extent RMSE. Thus, the calibrated Chang equation would be practical for large scale SWE mapping such as application to the entire Colorado River basin, as it requires a spatial interpolation of a single spatially coherent coefficient. Multiple TBD equations produced the most reliable estimates for at-site analysis, but their skill deteriorated when the analysis area increased; therefore, the equations require a regional approach similar to the procedure presented in Chapter 3. Statistical postprocessing did not reduce RMSE for both calibrated algorithms.

As a conclusive remark, the key idea of large scale SWE mapping over the mountainous regions is presented here. For both mapping approaches, it is more challenging to estimate SWE during snow ablation periods than during snow accumulation periods. This is illustrated by an increase in errors for both mapping techniques,

as examined in this dissertation. It is obvious that separate algorithms need to be developed or a different predictor set included for each period. The main issue when mapping SWE distribution for subcontinental scale or greater is that at a particular time, some locations are in the snow ablation phase while snow continues to accumulate in other areas. Therefore, the identification of regions with similar snow accumulation and ablation patterns could be an important step in successful SWE mapping on such a large areal scale.

With recent improvements in numerical weather, climate and land surface models, as well as quality of satellite derived terrain data (e.g., land cover type, and percentage), more gridded climate and physiographic data became available. Despite uncertain accuracy, such gridded data can provide reasonable spatial variability, which is the most important factor in delineating homogeneous snow climate regions.

5.2 Future studies

Finally, some thoughts about future studies are presented here for each individual analysis. The extensions of the study on SNOTEL snowpack properties presented in Chapter 2 are listed as follows:

- In this dissertation, only 130 sites out of over 700 sites provided sufficiently long records for this analysis. As the number of SNOTEL sites increases every year and SD sensors are installed at more sites, more detailed analysis of spatial and temporal characteristics of mountain snowpack density will be feasible in the near future.
- Spatial distribution of climatological snowpack density could be futher analyzed. For example, regional interpolation methods presented in Chapter 3 could be tested to derive gridded climatological snowpack density.

Future works associated with Chapter 3 include the following:

- Since significant meteorological predictors of monthly SWE change are precipitation in most cases (i.e., region and month) and air temperature in fewer cases, the regression analysis that excludes solar radiation and wind speed data could be performed for individual years, and interannual variability of SWE distribution could be analyzed in the context of climate study.
- Other alternative regionalization techniques should also be explored. Among the considered clustering algorithms are hierarchical clustering algorithms such as wards algorithm, as well as Self-Organizing Mapping [SOM; *Kohonen*, 2001]. As different clustering algorithms result in different regionalization, it follows that errors of SWE estimates should be examined for each regionalization technique in order to reduce SWE estimate errors.
- In this analysis, only multiple linear regression analysis was used for spatial interpolation technique. More sophisticated techniques could improve the accuracy of SWE estimates. For example, nonlinear techniques which might be worthwhile exploring include a binary regression tree model or the Artificial Neural Network. In addition, kriging of the residual from the regional regression equation could improve RMSE of the climatological SWE estimate.
- To estimate real-time or finer temporal SWE grids, the Mountain-Mapper technique could be tested using the developed monthly climatological SWE grids. Estimate errors from the Mounain-Mapper could be evaluated and compared to other interpolation methods proposed by *Fassnacht et al.* [2003]

Finally, more studies on passive microwave SWE retrieval algorithm will be needed to develop the algorithm towards an ability of deriving spatially continuous SWE.

- As aforementioned, calibration of multiple TBD equations need to be performed over the subregions of the Colorado River basin. Therefore, a regionalization scheme according to similar snow pack climate and physiographic characteris-

tics, which in tern affect passive microwave emission, needs to be investigated. This includes investigation of attribute variable selection, as well as regionalization schemes. The effect of regionalization on the SWE estimate error needs to be evaluated with an approach similar to the error analysis performed in Chapter 3.

- It is interesting to examine the spatial interpolation of the at-site calibrated coefficient of the Chang equation, as well as the effect of the interpolation methods on the error of the SWE estimate.
- Chapter 4 focused on the Colorado River basin where seasonal snowpack is characterized by lower density snowpack, as indicated in the results of Chapter 2. The ability of passive microwave data to retrieve SWE values over a maritime climate such as the Northwest Pacific area and Sierra Nevada needs to be explored.

APPENDIX

SNOTEL QUALITY CONTROL

The procedure to screen SNOTEL daily data (SWE and SD) was adopted from those used by *Serreze et al.* [1999] on SWE data. SWE and SD are reported as cumulative values rounded to the nearest 2.54 mm, starting on October 1. First, all negative SWE and SD values were eliminated from the records. Next, the SWE (SD) increment for day (i) was computed as a difference between SWE (SD) measurements on day (i+1) and day (i). Daily increments with an absolute value greater than 100 cm were removed from the dataset. Occasionally, very large positive SWE (SD) increments followed by large negative values (or the other way around) were identified. Those values were also considered erroneous and removed. Negative increments with an absolute value greater than five standard deviations from the average monthly negative daily increment for a given month were also removed from data sets. Similarly, positive increments greater than five standard deviations from the average monthly positive daily increment were also flagged and without the corresponding significant precipitation event were deleted from the datasets. Additionally, if the daily ratio of SWE to SD was less than 0.03 (lower limit of typical snow pack density; *McClung and Schaerer* [1993]) or more than one, both values were not included in the analysis.

REFERENCES

ACIA (2005), *Arctic climate impact assessment:scientific report*, 1042 pp., Cambridge University Press, Cambridge, United Kingdom.

Akitaya, E. (1974), Studies on depth hoar, *Tech. rep.*, Institute of Low Temperature Science, Hokkaido University.

Anagnostou, E. N., A. J. Negri, and R. F. Adler (1999), Statistical adjustment of satellite microwave monthly rainfall estimates over Amazonia, *Journal of Applied Meteorology*, *38*(11), 1590–1598, doi:10.1175/1520-0450(1999)038<1590:SAOSMM>2.0.CO;2.

Anderson, E. A. (1976), *A point energy and mass balance model of a snow cover*, 150 pp., U.S. Dept. of Commerce, National Oceanic and Atmospheric Administration, National Weather Service.

Anderton, S. P., S. M. White, and B. Alvera (2004), Evaluation of spatial variability in snow water equivalent for a high mountain catchment, *Hydrological Processes*, *18*, 435–453, doi:10.1002/hyp.1319.

Armstrong, R. L. (1980), An analysis of compressive strain in adjacent temperature-gradient and equi-temperature layers in a natural snow cover, *Journal of Glaciology*, *26*(94), 283–289.

Armstrong, R. L., and M. J. Brodzik (1995), An earth-gridded SSM/I data set for cryospheric studies and global change monitoring, *Advances in Space Research*, *16*(10), 155–163, doi:10.1016/0273-1177(95)00397-W.

Balk, B., and K. Elder (2000), Combining binary decision tree and geostatistical methods to estimate snow distribution in a mountain watershed, *Water Resources Research*, *36*(1), 13–26, doi:10.1029/1999WR900251.

Barrett, A. (2003), National operational hydrologic remote sensing center snow data assimilation system (SNODAS) products at NSIDC, NSIDC Special Report.

Billings, W. (1988), *Alpine vegetation*, pp. 391–420, Cambridge University Press, Cambridge, U. K.

Blöschl, G. (1999), Scaling issues in snow hydrology, *Hydrological Processes*, *13*, 2149–2175, doi:10.1002/(sici)1099-1085(199910)13:14/15<2149::aid-hyp847>3.0.co;2-8.

Brown, R., B. Brasnett, and D. Robinson (2003), Gridded North American monthly snow depth and snow water equivalent for GCM evaluation, *Atmosphere-Ocean*, *41*(1), 1–14, doi:10.3137/ao.410101.

Campbell, J., M. Mitchell, P. Groffman, L. Christenson, and J. Hardy (2005), Winter in northeastern North America: a critical period for ecological processes, *Frontiers in Ecology and Environment*, *3*(6), 314–322.

Carroll, S. S., and N. Cressie (1997), Spatial modeling of snow water equivalent using covariances estimated from spatial and geomorphic attributes, *Journal of Hydrology*, *190*(1-2), 42–59, doi:10.1016/S0022-1694(96)03062-4.

Carroll, T. R. (2001), *Airborne gamma radiation snow survey program: a user's guide : version 5.0*, 14 p. pp., National Operational Hydrologic Remote Sensing Center, National Weather Service, National Oceanic and Atmospheric Administration, U.S. Dept. of Commerce, Minneapolis, Minn.

Cayan, D. R. (1996), Interannual climate variability and snowpack in the western United States, *Journal of Climate*, *9*(5), 928–948, doi:10.1175/1520-0442(1996)009<0928:ICVASI>2.0.CO;2.

Chang, A. T. C., J. L. Foster, and D. K. Hall (1987), Nimbus-7 smmr derived global snow cover parameter, *Annals of Glaciology*, *9*, 39–44.

Chang, A. T. C., J. L. Foster, and D. K. Hall (1996), Effects of forest on the snow parameters derived from microwave measurements during the BOREAS winter field campaign, *Hydrological Processes*, *10*(12), 1565–1574, doi:10.1002/(sici)1099-1085(199612)10:12<1565::aid-hyp501>3.0.co;2-5.

Chang, A. T. C., J. L. Foster, R. E. J. Kelly, E. G. Josberger, R. L. Armstrong, and N. M. Mognard (2005), Analysis of ground-measured and passive-microwave-derived snow depth variations in midwinter across the northern Great Plains, *Journal of Hydrometeorology*, *6*(1), 20–33, doi:10.1175/JHM-405.1.

Cline, D., et al. (2009), NASA Cold Land Processes Experiment (CLPX 2002/03): Airborne remote sensing, *Journal of Hydrometeorology*, *10*(1), 338–346, doi: 10.1175/2008JHM883.1.

Cohen, J., and D. Entekhabi (1999), Eurasian snow cover variability and northern hemisphere climate predictability, *Geophysical Research Letter*, *26*(3), 345–348, doi:10.1029/1998gl900321.

Cohen, J., and D. Rind (1991), The effect of snow cover on the climate, *Journal of Climate*, *4*(7), 689–706, doi:10.1175/1520-0442(1991)004<0689:TEOSCO>2.0.CO;2.

Colbeck, S. (1997), *A review of sintering in seasonal snow*, 91-16 pp., U.S. Army Cold Region Research and Engineering Laboratory.

Colbeck, S. C. (1982), An overview of seasonal snow metamorphism, *Review of Geophysics*, *20*(1), 45–61, doi:10.1029/RG020i001p00045.

Dalrymple, T. (1960), *Flood frequency analyses, manual of hydrology*, 1543-A, USGS.

Daly, C., R. P. Neilson, and D. L. Phillips (1994), A statistical-topographic model for mapping climatological precipitation over mountainous terrain, *Journal of Applied Meteorology*, *33*(2), 140–158, doi:10.1175/1520-0450(1994)033<0140:ASTMFM>2.0.CO;2.

Daly, C., M. Halbleib, J. I. Smith, W. P. Gibson, M. K. Doggett, G. H. Taylor, J. Curtis, and P. P. Pasteris (2008), Physiographically sensitive mapping of climatological temperature and precipitation across the conterminous United States, *International Journal of Climatology*, *28*, 2031–2064, doi:10.1002/joc.1688.

Daly, S. F., R. Davis, E. Ochs, and T. Pangburn (2000), An approach to spatially distributed snow modelling of the Sacramento and San Joaquin basins, California, *Hydrological Processes*, *14*, 3257–3271, doi:10.1002/1099-1085(20001230)14:18<3257::aid-hyp199>3.0.co;2-z.

Decker, K., D. Wang, C. Waite, and T. Scherbatskoy (2003), Snow removal and ambient air temperature effects on forest soil temperatures in northern Vermont, *Soil Science Society of America Journal*, *67*(4), 1234–1242.

Derksen, C., A. Walker, and B. Goodison (2003), A comparison of 18 winter seasons of in situ and passive microwave-derived snow water equivalent estimates in western Canada, *Remote Sensing of Environment*, *88*(3), 271–282, doi:10.1016/j.rse.2003.07.003.

Dewey, K. F. (1977), Daily maximum and minimum temperature forecasts and the influence of snow cover, *Monthly Weather Review*, *105*(12), 1594–1597, doi:10.1175/1520-0493(1977)105<1594:DMAMTF>2.0.CO;2.

Di Luzio, M., G. L. Johnson, C. Daly, J. K. Eischeid, and J. G. Arnold (2008), Constructing retrospective gridded daily precipitation and temperature datasets for the conterminous United States, *Journal of Applied Meteorology and Climatology*, *47*(2), 475–497, doi:10.1175/2007JAMC1356.1.

Dong, J., J. P. Walker, and P. R. Houser (2005), Factors affecting remotely sensed snow water equivalent uncertainty, *Remote Sensing of Environment*, *97*(1), 68–82, doi:10.1016/j.rse.2005.04.010.

Dong, J., M. Ek, B. Cosgrove, V. Koren, H. Lee, M. Smith, P. Restrepo, and K. Mitchell (2011), High spatial resolution hydrological modeling on the hydrologic rainfall analysis project, in *paper presented at AMS 25th Conference on Hydrology*, Seattle, WA.

Dozier, J., and J. Frew (1990), Rapid calculation of terrain parameters for radiation modeling from digital elevation data, *Geoscience and Remote Sensing, IEEE Transactions on*, *28*(5), 963–969, doi:10.1109/36.58986.

Dozier, J., and T. H. Painter (2004), Multispectral and hyperspectral remote sensing of alpine snow properties, *Annual Review of Earth and Planetary Sciences*, *32*(1), 465–494, doi:10.1146/annurev.earth.32.101802.120404.

Dressler, K. A., G. H. Leavesley, R. C. Bales, and S. R. Fassnacht (2006), Evaluation of gridded snow water equivalent and satellite snow cover products for mountain basins in a hydrologic model, *Hydrological Processes*, *20*, 673–688, doi:10.1002/hyp.6130.

Dunne, T., and L. Leopold (1978), *Snow hydrology*, chap. 13, pp. 465–488, W.H. Freeman, New York.

Dyer, J. (2008), Snow depth and streamflow relationships in large North American watersheds, *Journal of Geophysical Research*, *113*(D18), D18,113, doi: 10.1029/2008jd010031.

Elder, K., W. Rosenthal, and R. E. Davis (1998), Estimating the spatial distribution of snow water equivalence in a montane watershed, *Hydrological Processes*, *12*, 1793–1808, doi:10.1002/(sici)1099-1085(199808/09)12:10/11<1793::aid-hyp695>3.0.co;2-k.

Erickson, T. A., M. W. Williams, and A. Winstral (2005), Persistence of topographic controls on the spatial distribution of snow in rugged mountain terrain, Colorado, United States, *Water Resources Research*, *41*(4), W04,014, doi: 10.1029/2003wr002973.

Erxleben, J., K. Elder, and R. Davis (2002), Comparison of spatial interpolation methods for estimating snow distribution in the Colorado Rocky Mountains, *Hydrological Processes*, *16*, 3627–3649, doi:10.1002/hyp.1239.

Everitt, B., S. Landau, and M. Leese (2001), *Cluster analysis*, 4th ed., Edward Arnold.

Farmer, C. J. Q., T. A. Nelson, M. A. Wulder, and C. Derksen (2010), Identification of snow cover regimes through spatial and temporal clustering of satellite microwave brightness temperatures, *Remote Sensing of Environment*, *114*(1), 199–210, doi: 10.1016/j.rse.2009.09.002.

Fassnacht, S. R., and J. E. Derry (2010), Defining similar regions of snow in the Colorado River basin using self-organizing maps, *Water Resources Research*, *46*(4), W04,507, doi:10.1029/2009wr007835.

Fassnacht, S. R., K. A. Dressler, and R. C. Bales (2003), Snow water equivalent interpolation for the Colorado River basin from snow telemetry (SNOTEL) data, *Water Resources Research*, *39*(8), 1208, doi:10.1029/2002wr001512.

Flanner, M. G., and C. S. Zender (2006), Linking snowpack microphysics and albedo evolution, *Journal of Geophysical Research*, *111*(D12), D12,208, doi: 10.1029/2005jd006834.

Foster, J. L., A. T. C. Chang, and D. K. Hall (1997), Comparison of snow mass estimates from a prototype passive microwave snow algorithm, a revised algorithm and a snow depth climatology, *Remote Sensing of Environment*, *62*(2), 132–142, doi:10.1016/S0034-4257(97)00085-0.

Foster, J. L., C. Sun, J. P. Walker, R. Kelly, A. Chang, J. Dong, and H. Powell (2005), Quantifying the uncertainty in passive microwave snow water equivalent observations, *Remote Sensing of Environment*, *94*(2), 187–203, doi: 10.1016/j.rse.2004.09.012.

Foster, J. L., D. K. Hall, R. E. J. Kelly, and L. Chiu (2009), Seasonal snow extent and snow mass in south america using SMMR and SSM/I passive microwave data (1979-2006), *Remote Sensing of Environment*, *113*(2), 291–305, doi:10.1016/j.rse.2008.09.010.

Fovell, R. G. (1997), Consensus clustering of U.S. temperature and precipitation data, *Journal of Climate*, *10*(6), 1405–1427, doi:10.1175/1520-0442(1997)010<1405:CCOUST>2.0.CO;2.

Fovell, R. G., and M.-Y. C. Fovell (1993), Climate zones of the conterminous United States defined using cluster analysis, *Journal of Climate*, *6*(11), 2103–2135, doi:10.1175/1520-0442(1993)006<2103:CZOTCU>2.0.CO;2.

Gan, T. Y., O. Kalinga, and P. Singh (2009), Comparison of snow water equivalent retrieved from SSM/I passive microwave data using artificial neural network, projection pursuit and nonlinear regressions, *Remote Sensing of Environment*, *113*(5), 919–927, doi:10.1016/j.rse.2009.01.004.

García-Herrera, R., and D. Barriopedro (2006), Northern Hemisphere snow cover and atmospheric blocking variability, *Journal of Geophysical Research*, *111*(D21), D21,104, doi:10.1029/2005jd006975.

Garen, D. C., and D. Marks (2005), Spatially distributed energy balance snowmelt modelling in a mountainous river basin: estimation of meteorological inputs and verification of model results, *Journal of Hydrology*, *315*(1-4), 126–153, doi:10.1016/j.jhydrol.2005.03.026.

Ge, Y., and G. Gong (2009), North American snow depth and climate teleconnection patterns, *Journal of Climate*, *22*(2), 217–233, doi:10.1175/2008JCLI2124.1.

Ge, Y., and G. Gong (2010), Land surface insulation response to snow depth variability, *Journal of Geophysical Research*, *115*(D8), D08,107, doi:10.1029/2009jd012798.

Goïta, K., A. E. Walker, and B. E. Goodison (2003), Algorithm development for the estimation of snow water equivalent in the boreal forest using passive microwave data, *International Journal of Remote Sensing*, *24*(5), 1097 – 1102, doi:10.1080/0143116021000044805.

Gong, G., D. Entekhabi, and J. Cohen (2002), A large-ensemble model study of the wintertime AO-NAO and the role of interannual snow perturbations, *Journal of Climate*, *15*(23), 3488–3499, doi:10.1175/1520-0442(2002)015<3488:ALEMSO>2.0.CO;2.

Gong, G., D. Entekhabi, and J. Cohen (2003), Modeled Northern Hemisphere winter climate response to realistic Siberian snow anomalies, *Journal of Climate*, *16*(23), 3917–3931, doi:10.1175/1520-0442(2003)016<3917:MNHWCR>2.0.CO;2.

Goodison, B., and A. E. Walker (1995), *Canadian development and use of snowcover information from passive microwave satellite data*, pp. 245–262, VSP Books.

Goodison, B., H. Ferguson, and G. Mckay (1981), *Measurement and data analysis*, pp. 191 – 274, Pergamon Press, Toronto.

Grant, L., and J. Rhea (1974), Elevation and meteorological controls on the density of snow, in *Advanced concepts and techniques in the study of snow and ice resource*, pp. 196–181, National Academy of Science.

Grippa, M., N. Mognard, T. Le Toan, and E. G. Josberger (2004), Siberia snow depth climatology derived from SSM/I data using a combined dynamic and static algorithm, *Remote Sensing of Environment*, *93*(1-2), 30–41, doi: 10.1016/j.rse.2004.06.012.

Groffman, P., C. Driscoll, T. Fahey, J. Hardy, R. Fitzhugh, and G. Tierney (2001), Colder soils in a warmer world: a snow manipulation study in a northern hardwood forest ecosystem, *Biogeochemistry*, *56*(2), 135–150, doi:10.1023/a:1013039830323.

Hall, D., A. T. C. Chang, and J. L. Foster (1986), Detection of the depth hoar layer in the snowpack of the arctic coastal plain of Alaska using satellite data, *Journal of Glaciology*, *32*(94), 87–94.

Hall, R., and F. Hannaford, J (1983), Analysis of three rain on snow floods in the Sierra Nevada, California, in *paper presented at Western Snow Conference*, vol. 51, pp. 46–54.

Hatch, D. (2006), Distribution of snow water equivalent climatology for the western united states from snow telemetry (snotel) data, Ph.D. thesis, University of Utah.

Hollinger, J. P., J. L. Peirce, and G. A. Poe (1990), SSM/I instrument evaluation, *Geoscience and Remote Sensing, IEEE Transactions on*, *28*(5), 781–790, doi:10.1109/36.58964.

Hosang, J., and K. Dettwiler (1991), Evaluation of a water equivalent of snow cover map in a small catchment area using a geostatistical approach, *Hydrological Processes*, *5*, 283–290, doi:10.1002/hyp.3360050308.

Jin, J., N. L. Miller, S. Sorooshian, and X. Gao (2006), Relationship between atmospheric circulation and snowpack in the western usa, *Hydrological Processes*, *20*, 753–767, doi:10.1002/hyp.6126.

Jordan, R. (1991), *A one-dimensional temperature model for a snow cover*, 91-16 pp., U. S. Army Cold Region Research and Engineering Laboratory.

Josberger, E. G., and N. M. Mognard (2002), A passive microwave snow depth algorithm with a proxy for snow metamorphism, *Hydrological Processes*, *16*, 1557–1568, doi:10.1002/hyp.1020.

Josberger, E. G., P. Gloersen, A. Chang, and A. Rango (1996), The effects of snowpack grain size on satellite passive microwave observations from the upper colorado river basin, *Journal of Geophysical Research*, *101*(C3), 6679–6688, doi: 10.1029/95jc02959.

Judson, A., and N. Doesken (2000), Density of freshly fallen snow in the central rocky mountains, *Bulletin of the American Meteorological Society*, *81*(7), 1577–1587, doi: 10.1175/1520-0477(2000)081<1577:DOFFSI>2.3.CO;2.

Kaempfer, T. U., and M. Schneebeli (2007), Observation of isothermal metamorphism of new snow and interpretation as a sintering process, *Journal of Geophysical Research*, *112*(D24), D24,101, doi:10.1029/2007jd009047.

Kalkstein, L. S., G. Tan, and J. A. Skindlov (1987), An evaluation of three clustering procedures for use in synoptic climatological classification, *Journal of Climate and Applied Meteorology*, *26*(6), 717–730, doi:10.1175/1520-0450(1987)026<0717:AEOTCP>2.0.CO;2.

Kelly, R., A. T. C. Chang, L. Tsang, and J. L. Foster (2003), A prototype AMSR-E global snow area and snow depth algorithm, *IEEE Transactions on Geoscience and Remote Sensing*, *41*(2), 230–242, doi:10.1109/TGRS.2003.809118.

Kelly, R. E. J., and A. T. C. Chang (2003), Development of a passive microwave global snow depth retrieval algorithm for Special Sensor Microwave Imager (SSM/I) and Advanced Microwave Scanning Radiometer-EOS (AMSR-E) data, *Radio Science*, *38*(4), 8076, doi:10.1029/2002rs002648.

Koenig, L. S., and R. R. Forster (2004), Evaluation of passive microwave snow water equivalent algorithms in the depth hoar-dominated snowpack of the kuparuk river watershed, alaska, usa, *Remote Sensing of Environment*, *93*(4), 511–527, doi:10.1016/j.rse.2004.08.004.

Kohonen, T. (2001), *Self-organizing maps*, 501 pp., Springer, New York.

Kojima, K. (1967), Densification of seasonal snow cover, institute of Low Temperature Science, Hokkaido University.

Kumar, L., A. Skidmore, and E. Knowles (1997), Modelling topographic variation in solar radiation in a GIS environment, *International Journal of Geographical Information Science*, *11*, 475–497.

LaChapelle, E. (1962), The density distribution of new snow. progress report. 2.

Lammers, R. B., A. I. Shiklomanov, C. J. Vörösmarty, B. M. Fekete, and B. J. Peterson (2001), Assessment of contemporary arctic river runoff based on observational discharge records, *Journal Geophysical Research*, *106*(D4), 3321–3334, doi:10.1029/2000jd900444.

Langham, E. (1981), *Physics and properties of snowcover*, pp. 275–337, Pergamon Press, Toronto.

Leathers, D. J., and D. Robinson (1993), The association between extremes in North American snow cover extent and United States temperatures, *Journal of Climate*, *6*(7), 1345–1355, doi:10.1175/1520-0442(1993)006<1345:TABEIN>2.0.CO;2.

Leathers, D. J., D. R. Kluck, and S. Kroczynski (1998), The severe flooding event of January 1996 across north-central Pennsylvania, *Bulletin of the American Meteorological Society*, *79*(5), 785–797, doi:10.1175/1520-0477(1998)079<0785:TSFEOJ>2.0.CO;2.

Li, H., J. Sheffield, and E. F. Wood (2010), Bias correction of monthly precipitation and temperature fields from intergovernmental panel on climate change ar4 models using equidistant quantile matching, *Journal of Geophysical Research*, *115*(D10), D10,101, doi:10.1029/2009jd012882.

MacQueen, J. (1967), Some methods for classification and analysis of multivariate observations, in *The Fifth Berkeley Symposium on Mathematical Statistics and Probability*, vol. 1, edited by L. Le Cam and J. Neyman, pp. 281–297, University of California Press.

Maeno, N., and T. Ebinuma (1983), Pressure sintering of ice and its implication to the densification of snow at polar glaciers and ice sheets, *The Journal of Physical Chemistry*, *87*(21), 4103–4110, doi:10.1021/j100244a023.

Marks, D., and J. Dozier (1992), Climate and energy exchange at the snow surface in the Alpine Region of the Sierra Nevada 2. Snow cover energy balance, *Water Resources Research*, *28*(11), 3043–3054, doi:10.1029/92WR01483.

Marks, D., J. Kimball, D. Tingey, and T. Link (1998), The sensitivity of snowmelt processes to climate conditions and forest cover during rain-on-snow: a case study of the 1996 pacific northwest flood, *Hydrological Processes*, *12*, 1569–1587, doi:10.1002/(sici)1099-1085(199808/09)12:10/11<1569::aid-hyp682>3.0.co;2-l.

Massom, R. A., et al. (2001), Snow on Antarctic sea ice, *Review of Geophysics*, *39*(3), 413–445, doi:10.1029/2000rg000085.

McCabe, G. J., and M. D. Dettinger (2002), Primary modes and predictability of year-to-year snowpack variations in the western United States from teleconnections with Pacific Ocean climate, *Journal of Hydrometeorology*, *3*(1), 13–25, doi:10.1175/1525-7541(2002)003<0013:PMAPOY>2.0.CO;2.

McClung, D., and P. Schaerer (1993), *The avalanche handbook*, 265 pp., The Mountaineers, Seattle, Washington.

McGurk, B., D. Azuma, and R. Kattelmann (1988), Density of new snow in the central Sierra Nevada, in *paper presented at Western Snow Conference*, vol. 69, pp. 158–161.

Mesinger, F., et al. (2006), North American regional reanalysis, *Bulletin of the American Meteorological Society*, *87*(3), 343–360, doi:10.1175/BAMS-87-3-343.

Mizukami, N., S. Perica, and D. Hatch (2011), Regional approach for mapping climatological snow water equivalent over the mountainous regions of the western United States, *Journal of Hydrology*, *400*(1-2), 72 – 82, doi:10.1016/j.jhydrol.2011.01.019.

Mölders, N., and J. E. Walsh (2004), Atmospheric response to soil-frost and snow in Alaska in March, *Theoretical and Applied Climatology*, *77*(1), 77–105, doi: 10.1007/s00704-003-0032-5.

Molotch, N. P., and R. C. Bales (2005), Scaling snow observations from the point to the grid element: implications for observation network design, *Water Resources Research*, *41*(11), W11,421, doi:10.1029/2005wr004229.

Molotch, N. P., and R. C. Bales (2006), SNOTEL representativeness in the Rio Grande headwaters on the basis of physiographics and remotely sensed snow cover persistence, *Hydrological Processes*, *20*, 723–739, doi:10.1002/hyp.6128.

Moreno, J. I. L., J. Latron, and A. Lehmann (2010), Effects of sample and grid size on the accuracy and stability of regression-based snow interpolation methods, *Hydrological Processes*, *24*, 1914–1928, doi:10.1002/hyp.7564.

Mote, P. W. (2006), Climate-driven variability and trends in mountain snowpack in western North America, *Journal of Climate*, *19*(23), 6209–6220, doi: 10.1175/JCLI3971.1.

Mote, P. W., A. F. Hamlet, M. P. Clark, and D. P. Lettenmaier (2005), Declining mountain snowpack in western North America, *Bulletin of the American Meteorological Society*, *86*(1), 39–49, doi:10.1175/BAMS-86-1-39.

Mote, T. L., A. J. Grundstein, D. J. Leathers, and D. A. Robinson (2003), A comparison of modeled, remotely sensed, and measured snow water equivalent in the northern Great Plains, *Water Resources Research*, *39*(8), 1209, doi: 10.1029/2002wr001782.

Nelson, B. R., D.-J. Seo, and D. Kim (2010), Multisensor precipitation reanalysis, *Journal of Hydrometeorology*, *11*(3), 666–682, doi:10.1175/2010JHM1210.1.

Palmer, P. (1988), The SCS snow survey water supply forecasting program: current operations and future directions, in *paper presented at Western Snow Conference*, vol. 56, pp. 43–51.

Pan, M., et al. (2003), Snow process modeling in the North American Land Data Assimilation System (NLDAS): 2. Evaluation of model simulated snow water equivalent, *Journal of Geophysical Research*, *108*(D22), doi:10.1029/2003JD003994.

Papamichail, D. M., and I. G. Metaxa (1996), Geostatistical analysis of spatial variability of rainfall and optimal design of a rain gauge network, *Water Resources Management*, *10*(2), 107–127, doi:107-127.10.1007/bf00429682.

Pulliainen, J., and M. Hallikainen (2001), Retrieval of regional snow water equivalent from space-borne passive microwave observations, *Remote Sensing of Environment*, *75*(1), 76–85, doi:10.1016/S0034-4257(00)00157-7.

Ramsay, B. H. (1998), The Interactive Multisensor Snow and Ice Mapping System, *Hydrological Processes*, *12*(10-11), 1537–1546, doi:10.1002/(sici)1099-1085(199808/09)12:10/11<1537::aid-hyp679>3.0.co;2-a.

Rango, A., A. T. C. Chang, and J. L. Foster (1979), Utilization of spaceborne microwave radiometers for monitoring snowpack properties, *Nordic Hydrology*, *10*(1), 25–40, doi:10.2166/nh.1979.003.

Regonda, S. K., B. Rajagopalan, M. Clark, and J. Pitlick (2005), Seasonal cycle shifts in hydroclimatology over the western United States, *Journal of Climate*, *18*(2), 372–384, doi:10.1175/JCLI-3272.1.

Reichle, R. H., and R. D. Koster (2004), Bias reduction in short records of satellite soil moisture, *Geophysical Research Letter*, *31*(19), L19,501, doi:10.1175/JCLI-3272.1.

Rutter, N., D. Cline, and L. Li (2009), Evaluation of the NOHRSC snow model (NSM) in a one dimensional model, *Journal of Hydrometeorology*, *9*, 695–711, doi: 10.1175/2008JHM861.1.

Saito, K., and J. Cohen (2003), The potential role of snow cover in forcing interannual variability of the major Northern Hemisphere mode, *Geophysical Research Letter*, *30*(6), doi:10.1029/2002GL016341.

Saunders, M. A., B. Qian, and B. Lloyd-Hughes (2003), Summer snow extent heralding of the winter North Atlantic Oscillation, *Geophysical Research Letter*, *30*(7), L1378, doi:10.1029/2002gl016832.

Schaake, J., A. Henkel, and S. Cong (2004), Application of PRISM climatologies for hydrologic modeling and forecasting in the western U.S, in *paper presented at AMS 18th Conference on Hydrology*, Seattle, WA.

Schaefer, G., and D. Johnson (1992), Development and operation of the SNOTEL system in the western United States, in United States/People's Republic of China Flood Forecasting Symposium, Portland Oregon.

Serreze, M. C., M. P. Clark, R. L. Armstrong, D. A. McGinnis, and R. S. Pulwarty (1999), Characteristics of the western United States snowpack from snowpack telemetry (SNOTEL) data, *Water Resources Research*, *35*(7), 2145–2160, doi: 10.1029/1999wr900090.

Singh, P. R., and T. Y. Gan (2000), Retrieval of snow water equivalent using passive microwave brightness temperature data, *Remote Sensing of Environment*, *74*(2), 275–286, doi:10.1016/S0034-4257(00)00121-8.

Sobolowski, S., and A. Frei (2007), Lagged relationships between North American snow mass and atmospheric teleconnection indices, *International Journal of Climatology*, *27*, 221–231, doi:10.1002/joc.1395.

Stewart, I. T., D. R. Cayan, and M. D. Dettinger (2005), Changes toward earlier streamflow timing across western North America, *Journal of Climate*, *18*(8), 1136–1155, doi:10.1175/JCLI3321.1.

Stieglitz, M., S. J. Déry, V. E. Romanovsky, and T. E. Osterkamp (2003), The role of snow cover in the warming of arctic permafrost, *Geophysical Research Letter*, *30*(13), 1721, doi:10.1029/2003gl017337.

Sturm, M., J. Holmgren, and G. E. Liston (1995), A seasonal snow cover classification system for local to global applications, *Journal of Climate*, *8*(5), 1261–1283, doi:10.1175/1520-0442(1995)008<1261:ASSCCS>2.0.CO;2.

Tait, A., and R. Armstrong (1996), Evaluation of SMMR satellite-derived snow depth using ground-based measurements, *International Journal of Remote Sensing*, *17*(4), 657 – 665, doi:10.1080/01431169608949036.

Tait, A. B. (1998), Estimation of snow water equivalent using passive microwave radiation data, *Remote Sensing of Environment*, *64*(3), 286–291, doi:10.1016/S0034-4257(98)00005-4.

Tedesco, M., J. Pulliainen, M. Takala, M. Hallikainen, and P. Pampaloni (2004), Artificial neural network-based techniques for the retrieval of SWE and snow depth from SSM/I data, *Remote Sensing of Environment*, *90*(1), 76–85, doi:10.1016/j.rse.2003.12.002.

Thyer, M., J. Beckers, D. Spittlehouse, Y. Alila, and R. Winkler (2004), Diagnosing a distributed hydrologic model for two high-elevation forested catchments based on detailed stand- and basin-scale data, *Water Resources. Research.*, *40*(1), W01,103, doi:10.1029/2003WR002414.

Tong, J., S. Dery, P. Jackson, and C. Derksen (2010), Testing snow water equivalent retrieval algorithms for passive microwave remote sensing in an alpine watershed of western Canada, *Canadian Journal of Remote Sensing*, *36*(1), 74–86, doi:10.5589/m10-009.

Ulaby, F., R. Moore, and A. Fung (1986), *Microwave remote sensing: active and passive*, *microwave remote sensing fundamentals and radiometry*, vol. 1, 456 pp., Addison-Wesley, Reading, Massachusetts.

United States Army Corps of Engineers (1956), *Snow hydrology: summary report of the snow investigations*, 437 pp., The Division, Portland, OR.

Šúri, M., and J. Hofierka (2004), A new GIS-based solar radiation model and its application to photovoltaic assessments, *Transactions in GIS*, *8*, 175–190, doi:10.1111/j.1467-9671.2004.00174.x.

Wagner, A. J. (1973), The influence of average snow depth on monthly mean temperature anomaly, *Monthly Weather Review*, *101*(8), 624–626, doi:10.1175/1520-0493(1973)101<0624:TIOASD>2.3.CO;2.

Walker, A., and B. Goodison (1993), Discrimination of a wet snow cover using passive microwave satellite data, *Annals of Glaciology*, *17*, 307–311.

Walker, D. A., J. C. Halfpenny, M. D. Walker, and C. A. Wessman (1993), Long-term studies of snow-vegetation interactions, *BioScience*, *43*(5), 287–301, articleType: research-article / Full publication date: May, 1993 / University of California Press and American Institute of Biological Sciences.

Walsh, J. E., and B. Ross (1988), Sensitivity of 30-day dynamical forecasts to continental snow cover, *Journal of Climate*, *1*(7), 739–754, doi:10.1175/1520-0442(1988)001<0739:SODDFT>2.0.CO;2.

Walsh, J. E., D. R. Tucek, and M. R. Peterson (1982), Seasonal snow cover and short-term climatic fluctuations over the United States, *Monthly Weather Review*, *110*(10), 1474–1486, doi:10.1175/1520-0493(1982)110<1474:SSCAST>2.0.CO;2.

Wilks, D. (2005), *Statistical methods in the atmospheric sciences*, 627 pp., Academic Press, San Diego, CA.

Williams, M. W., P. D. Brooks, and T. Seastedt (1998), Nitrogen and carbon soil dynamics in response to climate change in a high-elevation ecosystem in the Rocky Mountains, U.S.A, *Arctic and Alpine Research*, *30*(1), 26–30.

Wood, A. W., E. P. Maurer, A. Kumar, and D. P. Lettenmaier (2002), Long-range experimental hydrologic forecasting for the eastern United States, *Journal Geophysical Research*, *107*(D20), 4429, doi:10.1029/2001JD000659.

Xue, Y., S. Sun, D. S. Kahan, and Y. Jiao (2003), Impact of parameterizations in snow physics and interface processes on the simulation of snow cover and runoff at several cold region sites, *Journal Geophysical Research*, *108*(D22), 8859, doi: 10.1029/2002JD003174.

Yang, D., D. Robinson, Y. Zhao, T. Estilow, and B. Ye (2003), Streamflow response to seasonal snow cover extent changes in large Siberian watersheds, *Journal Geophysical Research*, *108*(D18), 4578, doi:10.1029/2002JD003149.

Zhang, X., K. D. Harvey, W. D. Hogg, and T. R. Yuzyk (2001), Trends in Canadian streamflow, *Water Resources Research*, *37*(4), 987–998, doi: 10.1029/2000WR900357.